Durham University

Durham Research Online

Deposited in DRO:

30 January 2015

Version of attached file:

Accepted Version

Peer-review status of attached file:

Peer-reviewed

Citation for published item:

Horner, T. and Williams, H. and Hein, J. and Saito, M. and Burton, K. and Halliday, A. and Nielsen, S. (2015) 'Persistence of deeply sourced iron in the Pacific Ocean.', Proceedings of the National Academy of Sciences., 112 (05). pp. 1292-1297.

Further information on publisher's website:

http://dx.doi.org/10.1073/pnas.1420188112

Publisher's copyright statement:

Additional information:

Use policy

The full-text may be used and/or reproduced, and given to third parties in any format or medium, without prior permission or charge, for personal research or study, educational, or not-for-profit purposes provided that:

- a full bibliographic reference is made to the original source
- a link is made to the metadata record in DRO
- the full-text is not changed in any way

The full-text must not be sold in any format or medium without the formal permission of the copyright holders.

Please consult the full DRO policy for further details.

Durham University Library, Stockton Road, Durham DH1 3LY, United Kingdom
Tel : +44 (0)191 334 3042 | Fax : +44 (0)191 334 2971
https://dro.dur.ac.uk

Persistence of deeply sourced iron in the Pacific Ocean

Tristan J. Horner[a,1], Helen M. Williams[b,c,1], James R. Hein[d], Makoto A. Saito[a], Kevin W. Burton[b,c], Alex N. Halliday[c], and Sune G. Nielsen[a]

December 2, 2014

[a]Woods Hole Oceanographic Institution, MA 02543, USA; [b]Durham University, Durham DH1 3LE, UK; [c]University of Oxford, Oxford OX1 3AN, UK; [d]United States Geological Survey, Santa Cruz, CA 95060, USA

[1]To whom correspondence should be addressed. E-mail: Tristan.Horner@whoi.edu; h.m.williams2@durham.ac.uk

Classification PHYSICAL SCIENCES: Earth, Atmospheric, and Planetary Sciences

Keywords marine chemistry; micronutrient cycling; iron biogeochemistry; isotopic fingerprinting; ferromanganese oxides

Author contributions H.M.W., J.R.H., K.W.B., A.N.H., and S.G.N. designed research; H.M.W. and M.A.S. performed research; T.J.H. and S.G.N. analyzed data; and T.J.H. wrote the paper.

The authors declare no conflict of interest.

Abstract

Biological carbon fixation is limited by the supply of Fe in vast regions of the global ocean. Dissolved Fe in seawater is primarily sourced from continental mineral dust, submarine hydrothermalism, and sediment dissolution along continental margins. However, the relative contributions of these three sources to the Fe budget of the open ocean remains contentious. By exploiting the Fe stable isotopic fingerprints of these sources, it is possible to trace distinct Fe pools through marine environments, and through time using sedimentary records. We present a reconstruction of deep-sea Fe-isotopic compositions from a Pacific Fe-Mn crust spanning the past 76 Myr. We find that there have been large and systematic changes in the Fe-isotopic composition of seawater over the Cenozoic that reflect the influence of several, distinct Fe sources to the central Pacific Ocean. Given that deeply sourced Fe from hydrothermalism and marginal sediment dissolution exhibit the largest Fe-isotopic variations in modern oceanic settings, the record requires that these deep Fe sources have exerted a major control over the total Fe inventory of the Pacific for the past 76 Myr. The persistence of deeply sourced Fe in the Pacific Ocean illustrates that multiple sources contribute to the total Fe budget of the ocean and highlights the importance of oceanic circulation in determining if deeply sourced Fe is ever ventilated at the surface.

Significance

The vertical supply of dissolved Fe (iron) is insufficient compared to the physiological needs of marine phytoplankton in vast swathes of the open ocean. However, the relative importance of the main sources of 'new' Fe to the ocean – continental mineral dust, hydrothermal exhalations, and sediment dissolution – and their temporal evolution are poorly constrained. By analyzing the isotopic composition of Fe in marine sediments, we find that much of the dissolved Fe in the central Pacific Ocean originated from hydrothermal and sedimentary sources thousands of meters below the sea surface. As such, these data underscore the vital role of the oceans' physical mixing in determining if any deeply sourced Fe ever reaches the Fe-starved surface-dwelling biota.

Introduction

IRON (Fe) is the most abundant transition metal in marine phytoplankton, reflecting its importance for a range of biochemical processes such as photosynthesis and nitrogen fixation.[1] The high cellular requirements for Fe, coupled with its low solubility and concentrations in seawater, render Fe a limiting nutrient in vast regions of the global ocean.[2] In turn, this makes the availability of dissolved Fe a potential controlling factor for changes in atmospheric pCO_2 and thereby major oscillations in Earth's climate. Global biogeochemical models show that more regions of the surface ocean are dominated by circulation-driven dissolved Fe fluxes from below than by surface aerosol fluxes (e.g[3,4]). This upward flux of dissolved Fe is itself primarily sourced from three main pathways: dissolution of mineral dust (e.g.[5]), submarine hydrothermalism (e.g.[6–8]), and from sediment dissolution along continental margins (e.g.[9,10]), with the main removal mechanism being scavenging onto sinking particles (e.g.[11]). However, the significance of deeply-derived Fe sources – submarine sediment dissolution and hydrothermalism – compared with surface Fe sources (dust dissolution), remains controversial (e.g[12,13]). Given the key role of Fe in supporting oceanic primary production, quantifying the relative importance of the various Fe sources – both in the modern ocean and in the geological record – is critical to understanding how micronutrient cycles are related to Earth's climatic state.

One promising way to trace Fe sources in the modern ocean is with measurements of stable Fe-isotopic compositions, where $\delta^{56/54}\text{Fe} = \left({}^{56/54}\text{Fe}_{\text{sample}}/{}^{56/54}\text{Fe}_{\text{IRMM}-14} - 1\right) \times 1{,}000$. Recent studies showed that the Fe-isotopic composition of seawater is primarily controlled by the relative input of isotopically distinct Fe sources,[14–16] and that these source signatures can be transported and retained over thousands of kilometers within the ocean interior.[14] The large range in Fe-isotopic compositions observed between different Fe sources (≥ 4 ‰) and in seawater (> 2 ‰[14–18]) should therefore also be reflected in sedimentary archives that faithfully capture the Fe-isotopic composition of seawater.

Here, we report a record of $\delta^{56/54}$Fe from CD29-2, a mineralogically-uniform[19] Fe-Mn (ferromanganese) crust collected from the flank of the Karin Ridge at 16°42.4′ N, 168°14.2′ W in the central Pacific (;[20] Fig. 1). The present water depth of CD29-2 is $\approx 2{,}000$ m, though the depth at the time when Fe-Mn crust formation commenced was likely $\sim 1{,}000$ m (owing to thermal subsidence; see SI, Supporting Information). Hydrogenetic Fe-Mn crusts are irregularly layered sedimentary deposits that form through chemical precipitation of Fe- and Mn-oxides from ambient seawater, forming a mineral termed ferroxyhyte.[21] Their persistence on rocky substrates away from sediment sources that might bury the crust[21] allows other metals to adsorb and become incorporated into Fe-Mn crusts via lattice replacement or co-precipitation with Fe- or Mn-oxides.[22] Detailed elemental stratigraphy showed that CD29-2 is hydrogenetic – rather than hydrothermal or diagenetic – in origin.[19] This designation means that the Fe and other metals contained within CD29-2 were sourced from ambient seawater at the time of deposition, rather than diagenetic remobilization of sedimentary metals, or through accretion of hydrothermal vent-derived Fe- and Mn-oxides.

The extremely slow growth rate of most hydrogenetic deposits ($1 - 10$ mm Myr^{-1};[23]) renders Fe-Mn crusts as ideal recorders of long term changes in seawater trace element-isotopic chemistry. CD29-2 has an average growth rate of ≈ 1.4 mm Myr^{-1},[23] with each discrete sample for $\delta^{56/54}$Fe (between $0.2 - 0.5$ mm) integrating between $140 - 350$ kyr of Earth history. Since the residence time of dissolved Fe in the deep ocean (≈ 270 years[24]) is less than the mixing time of the oceans ($\approx 1{,}000$ years[25]), our record provides a 'local' history of the central Pacific, rather than of global seawater $\delta^{56/54}$Fe. Postdepositional processes such as diffusional re-equilibration with seawater[26] or precipitation of calcium fluorapatite in Fe-Mn crust pore spaces[27] have not affected the Fe-isotopic record in CD29-2 (see SI). Therefore, the

Figure 1: Map of sample locations. Sample CD29-2 was recovered from the flanks of the Karin Ridge at $\sim$ 2,000 m depth. CD29-2 is a semi-continuous hydrogenetic depositional record of many trace element isotopic compositions – including Fe – spanning the past $\approx$ 76 Ma (Fig. 3). The locations of other samples referred to throughout the text and in Fig. 4 are also shown: 28DSR9, a hydrogenetic Fe-Mn crust with a detailed Fe-isotopic stratigraphy for the past $\approx$ 10 Ma;[28] and DSDP (Deep Sea Drilling Project) Site 576[29] and LL44-GPC3,[30] two continuous Cenozoic records of aeolian deposition. Map drafted in Ocean Data View.[31]

Figure 2: Calculation of the Fe-isotopic offset between modern Fe-Mn crust surfaces and ambient seawater. (*A*) Fe-isotopic topology between Fe-Mn crusts (diamonds[33]) and the three nearest seawater stations (squares[16]). The thickness of the connecting line denotes the proximity ranking, with the thickest line linking each crust with its nearest corresponding seawater station, and so on. (*Fe-Mn crust 1966.069 was excluded from the offset calculation as there are no proximal seawater data, whereas seawater data from station TAG were excluded owing to their significant hydrothermal influence.) Values of $\Delta^{56/54}Fe_{FeMn-SW}$ were calculated by comparing the Fe-isotopic composition of the surface scraping of N. Atlantic Fe-Mn crusts with the Fe-isotopic composition of the corresponding density surface (σ_θ) at each seawater station, for each of the three picks. The uncertainty on each pick corresponds to the propagated 2 SD measurement uncertainty on Fe-Mn crust and seawater $\delta^{56/54}$Fe. Calculated $\Delta^{56/54}Fe_{FeMn-SW}$ compared against: (*B*) distance to nearest seawater station, (*C*) depth to corresponding density surface in the water column, and (*D*) ambient dissolved [Fe]. No relationship between $\Delta^{56/54}Fe_{FeMn-SW}$ and distance, depth, or [Fe] is evident from the data. The depths of the nine Fe-Mn crusts used in the offset calculation are shown in panel (*C*) as diamonds. The mean, unweighted fractionation factor is calculated as $\Delta^{56/54}Fe_{FeMn-SW} = -0.77 \pm 0.06$ ‰ (2 SE, $n = 27$) and is shown as the horizontal bar in panels (*B*)–(*D*). By assuming an invariant $\Delta^{56/54}Fe_{FeMn-SW}$ through time, it is possible to reconstruct the Fe-isotopic history of seawater from Fe-Mn crusts.

Fe-isotopic range of CD29-2 ($\delta^{56/54}$Fe $= -1.12$ to $+1.54$ ‰, with mean and median values of -0.02 and -0.04 ‰, respectively), must reflect primary depositional signatures inherited from Fe dissolved in seawater.

Estimating the Fe-isotopic fractionation factor, its driving mechanism, and variability through time

A robust reconstruction of the Fe-isotopic history of seawater from Fe-Mn crusts requires that the fractionation factor between Fe-Mn crusts and seawater, $\Delta^{56/54}Fe_{FeMn-SW}$, is accurately known, is unaffected by ambient environmental conditions, and has remained relatively constant through time. Stable isotopic offsets between Fe-Mn crusts and seawater are common for many elements, and likely result from differences in the relative binding strength between chemical species dissolved in seawater and incorporated in Fe-Mn crusts (e.g.[32]). We calculated the fractionation factor, defined as $\Delta^{56/54}Fe_{FeMn-SW} = \delta^{56/54}Fe_{FeMn} - \delta^{56/54}Fe_{SW}$, by comparing $\delta^{56/54}$Fe of the surface scrapings of nine N. Atlantic Fe-Mn crusts[33] with nearby seawater $\delta^{56/54}$Fe measurements from the recent US GEOTRACES North Atlantic GA03 Zonal Transect.[16] Each crust was compared with linearly interpolated seawater $\delta^{56/54}$Fe at the corresponding density surface for the three nearest seawater profiles (topology shown in Fig. 2a). The uncertainty on each estimate of $\Delta^{56/54}Fe_{FeMn-SW}$ refers to the propagated 2 SD external uncertainty as reported in the respective original publications. The mean, unweighted fractionation factor was calculated as $\Delta^{56/54}Fe_{FeMn-SW} = -0.77 \pm 0.06$ ‰ (2 SE, $n = 27$), and shows no obvious dependence on crust–seawater distance, sample depth, or ambient dissolved [Fe] (Figs. 2b, c, and d, respectively). We chose to report the uncertainty about the mean value as two standard errors owing to the remarkable coherence and unidirectional nature of calculated Fe-Mn crust–seawater offsets, as well as the large number of independent estimates of $\Delta^{56/54}Fe_{FeMn-SW}$ (Table 1).

The comparison of modern Fe-Mn crust growth surfaces and nearby ambient seawater indicates that Fe bound in Fe-Mn crusts is isotopically lighter than dissolved in seawater (Fig. 2), indicative of stronger

binding of Fe in seawater than in Fe-Mn crusts at equilibrium (e.g.[34]). Given the importance of siderophore-like strong Fe-binding ligands in stabilizing dissolved Fe in seawater,[35,36] it is extremely likely that organic ligands play an important – if not dominant – role in setting $\Delta^{56/54}Fe_{FeMn-SW}$. Several studies have documented that isotopically heavy Fe will preferentially associate with organic ligands during equilibration between aqueous Fe(III) and Fe–ligand complexes.[37–39] The binding strength of the Fe–ligand complex can modulate the magnitude of Fe-isotopic fractionation, with stronger ligands – and thus stronger bonding environments – favoring larger equilibrium Fe-isotopic fractionation factors. (Analogous behavior has also been identified for Cu,[40] which likely explains both the direction and magnitude of Cu-isotopic fractionation between Fe-Mn crusts and seawater.[41]) The calculated value of $\Delta^{56/54}Fe_{FeMn-SW}$ of -0.77 ± 0.06 ‰ is essentially identical to the empirically-determined $\Delta^{56/54}Fe_{Fe(III)-Fe(sid)}$ between inorganic dissolved Fe(III) and Fe–siderophore complexes of -0.60 ± 0.15 ‰.[37] The remarkable agreement between Fe-isotopic fractionation factors determined by experiments[37] and those observed between naturally occurring Fe-Mn crusts and seawater (Fig. 2) suggests that organic ligands may exert a dominant control on $\Delta^{56/54}Fe_{FeMn-SW}$.

Interpretation of Fe-Mn crust-derived records of seawater $\delta^{56/54}$Fe rely on $\Delta^{56/54}Fe_{FeMn-SW}$ having been constant through time. If ligands are indeed exerting a significant influence on Fe-isotopic fractionation in seawater, it is important to understand how evolutionary changes in the dominant Fe-binding ligands may have also affected $\Delta^{56/54}Fe_{FeMn-SW}$. To address this issue, we examined the evolutionary history of a component from each of two common siderophore biosynthetic pathways, as siderophores are thought to contribute to the oceanic Fe ligand inventory:[42] enterobactin synthase subunit F (EntF) and desferrioxamine E biosynthesis protein DesA. Whilst these are unlikely to be the only ligands in seawater, these ligands – and in particular, DFO (desferrioxamine) – are good analogues to other marine Fe ligands for several reasons: (1) The DFO class of ligands has been shown to exist in seawater;[43] (2) DFO possesses similar conditional Fe binding constants to natural marine Fe ligands;[44] and (3) The Fe-isotopic fractionation factor between dissolved Fe(III) and Fe–DFO complexes of $\Delta^{56/54}Fe_{Fe(III)-Fe(DFO)}$ of -0.60 ± 0.15 ‰[37] is identical to $\Delta^{56/54}Fe_{FeMn-SW}$, within uncertainty. Analysis of sequence alignments of the genes encoding these proteins in extant microbes demonstrates that siderophore biosynthesis genes diverged from a common ancestor well before the 76 Myr timespan of interest in this study (see SI). Given this finding, we contend that Fe-binding ligands have been present in seawater over the past 76 Myr, and likely far longer. Since the mineralogy of CD29-2 is invariant over this time period,[19] it follows that the differences in binding strength – and therefore the equilibrium $\Delta^{56/54}Fe_{FeMn-SW}$ – between ligand-stabilized Fe in seawater and Fe bound in CD29-2 has also remained constant for at least 76 Myr. Together with the observations that there are no resolvable Fe-isotopic effects related to Fe transport distance, water depth, or ambient [Fe] on $\Delta^{56/54}Fe_{FeMn-SW}$ in the modern ocean (Fig. 2), the use of a temporally-constant $\Delta^{56/54}Fe_{FeMn-SW}$ of -0.77 ± 0.06 ‰ for the past 76 Myr is justified by all available oceanographic, experimental, and genomic data.

Controls on the Fe-isotopic composition of seawater

It is worthwhile to briefly review what is currently known about the Fe-isotopic systematics of the major Fe sources to the modern ocean, as this information is used as the interpretive framework for understanding the seawater record contained within CD29-2. The Fe-isotopic composition of seawater is thought to be primarily controlled by the relative input of local, isotopically distinct Fe sources (Fig. 3a), modulated by secondary modification processes (Fig. 3a), and mixing by oceanic circulation.[14–16] The persistence of primary Fe-isotopic signatures along distinct water masses spanning thousands of kilometers suggests that the oceans' internal cycling of Fe through biological uptake and exchange with sinking

Figure 3: The Fe-isotopic history of central Pacific seawater over the past 76 Myr. (*A*) Fe-isotopic compositions of the major oceanic Fe fluxes. The bold lines represent the end-member compositions of each flux: continental crust, hydrothermal fluids, and non-reductive sediment dissolution. (A second end-member for reductive sediment dissolution ~ -3 ‰ is not shown; ref.[9]) Numerous processes have been shown to modify end-member Fe-isotopic compositions; the dashed lines illustrate the observed range of Fe-isotopic compositions for each flux resulting from secondary modification processes (see text for references and discussion). (*B*) An Fe-isotopic history of central Pacific seawater recovered from CD29-2 spanning the past 76 Ma. The solid line links the measurements in relative chronological order; the break in the solid line between 37 and 42 Ma signifies a probable hiatus in the crust growth.[23] The surface measurement ($\approx$ 0 Ma) is from Levasseur *et al.*[33] The gray and black error bars represent the analytical and propagated analytical and calculated uncertainties in $\Delta^{56/54}Fe_{FeMn-SW}$, respectively. The light-colored shading indicates the boundaries between relevant geological Epochs; colors as per.[45] Within each Epoch, measurements of $\delta^{56/54}$Fe have been binned, with the darker shading corresponding to one standard deviation either side of the mean value for that epoch. The shaded region labeled 'Modern' corresponds to the mean and standard deviation of the surfaces of globally distributed Fe-Mn crusts,[33] but has been expanded to cover the Quaternary for the sake of clarity.[33] (Pliocene and Micocene averages also include Fe-Mn crust data from Chu *et al.*;[28] see Fig. 4.) The greyed-out scale to the right of the figure shows the measured Fe-isotopic ratios for CD29-2 that have not been corrected for $\Delta^{56/54}Fe_{FeMn-SW} \approx -0.77$ ‰.

particles exert only minimal influences on dissolved $\delta^{56/54}$Fe.[14,16] As such, the Fe-isotopic composition of a water mass appears to be primarily governed by the Fe-isotopic composition of the dominant Fe source to that water mass, in addition to any source Fe-isotopic modification processes at the time of Fe addition. Iron-isotopic measurements can therefore be used to help elucidate the ultimate sources of Fe to the ocean, and in particular the deep open ocean, where the dominant sources of Fe are still hotly debated (e.g.[7,46–48]).

The end-member Fe-isotopic composition of the three major Fe sources to the open ocean – mineral aerosol or 'dust', seafloor sediment dissolution, and hydrothermalism – are summarized in Fig. 3a (bold lines). The major surface Fe source, dust, is characterized by $\delta^{56/54}Fe \approx +0.1 \pm 0.2$ ‰,[49] identical to the average Fe-isotopic composition of crustal rocks ($\delta^{56/54}Fe \approx +0.1 \pm 0.1$ ‰[50]). Deeply sourced Fe from dissolution of shelf sediments and hydrothermalism have distinct and variable Fe-isotopic compositions. Reductive dissolution of marginal sediments delivers isotopically light Fe to seawater, with $\delta^{56/54}Fe \sim -3.0$ ‰,[9] whereas non-reductive dissolution transfers Fe with a continental crust-like composition of $\delta^{56/54}Fe \approx +0.2 \pm 0.2$ ‰.[10] End-member hydrothermal fluid $\delta^{56/54}$Fe has been measured ≈ -0.2 ‰,[51,52] with a small but significant fraction of this Fe escaping precipitation and becoming stabilized in seawater as Fe(III).[7,47]

For each of these three major oceanic Fe fluxes, secondary modification processes have been shown to affect the Fe-isotopic composition of ligand-stabilized Fe in seawater (dashed lines in Fig. 3a). The Fe-isotopic composition of dust-derived Fe in seawater appears to be isotopically heavier than crustal rocks by $\approx +0.6$ ‰ at $\delta^{56/54}Fe \approx +0.7 \pm 0.1$ ‰(Fig. 3a;[16]). In the absence of ligands, total digests and leaching experiments on aerosol particulates have shown that Fe leached from dust possesses $\delta^{56/54}Fe \approx +0.1 \pm 0.2$ ‰.[49] The +0.6 ‰ offset between Fe bound in dust particles and dust-derived dissolved Fe in seawater is thought to result from the equilibrium isotopic partitioning of isotopically heavy Fe into strongly bound ligand-stabilized dissolved Fe(III) during dust dissolution.[16] This interpretation is consistent with experimental studies of Fe-isotopic fractionation during mineral dissolution[53] and during dissolved Fe(III)–ligand Fe-isotopic partitioning experiments.[38,39] Since Fe-binding organic ligands have an ancient biological origin that pre-dates the base of CD29-2 (see SI), it is likely that the Fe-isotopic offset between dust particles and ligand-stabilized dust-derived Fe in seawater ($\Delta^{56/54}Fe_{\text{dust part.}-\text{dust diss.}} \approx -0.6 \pm 0.2$ ‰[16,49,50]) has remained constant over the course of our 76 Myr record. It is worth noting that $\Delta^{56/54}Fe_{\text{dust part.}-\text{dust diss.}}$ and $\Delta^{56/54}Fe_{FeMn-SW}$ are identical, within uncertainty, lending further support to the notion that a common ligand-mediated mechanism controls both Fe-isotopic offsets.

For deep Fe sources – hydrothermalism and sediment dissolution – Fe-isotopic modification processes have also been identified, though the mechanisms involved are different than for mineral aeorsol Fe-isotopic modification. The most important modification processes identified in deep settings is the precipitation of dissolved Fe in either oxide or sulfide forms, depending on local seawater conditions. These two Fe-precipitating pathways impart large and distinct Fe-isotopic fractionations of opposite signs, as Fe-oxides generally favor precipitation of isotopically heavy Fe (i.e. $\Delta^{56/54}Fe_{oxide-dissolved} > 0$;[51]) and Fe-sulfides exclusively favor incorporation of isotopically light Fe (i.e. $\Delta^{56/54}Fe_{sulfide-dissolved} < 0$.[54–56]). Residual, dissolved Fe will thus become isotopically heavier as a result of Fe-sulfide precipitation, and isotopically lighter as a result of Fe-oxide precipitation. Field studies have shown that Fe-sulfide precipitation in continental margin sediments[10,55] and at hydrothermal vent sites[52,57] can drive the Fe-isotopic composition of residual Fe, and thereby deep water Fe fluxes, toward heavier $\delta^{56/54}$Fe by over +2 ‰[58] compared to the end-member compositions (Fig. 3a). Furthermore, formation of isotopically heavy Fe-oxide precipitates around hydrothermal vents has also been shown to drive the delivery of isotopically light Fe to the deep ocean (e.g.[16,51]).

Given the large range of Fe-isotopic variability between different Fe sources (Fig. 3a) and observed in the modern ocean,[14–17] we should naturally expect that changes in the dominant sources of Fe to the ocean with time will be accompanied by large shifts in the Fe-isotopic composition of seawater. Shifts in seawater $\delta^{56/54}$Fe with time will thus depend on the relative input of different Fe sources to the ocean *and* the extent of their modification prior to stabilization in seawater (Fig. 3).

An Fe-isotopic history of central Pacific seawater

Examination of our record of $\delta^{56/54}$Fe reveals large changes in the Fe-isotopic composition of central Pacific seawater over the past 76 Myr (Fig. 3b). Though much of the record lies outside of the field defined by source 'end-member' $\delta^{56/54}$Fe (Fig. 3a), when the aforementioned source modification processes are taken into account, even the most extreme $\delta^{56/54}$Fe values in the Oligocene fall within the Fe-isotopic range defined by modern Fe fluxes (Fig. 3). Overall, the Fe-isotopic record of seawater reveals significant temporal variability, which suggests that the dominant Fe sources to the ocean have also varied over time, and that multiple Fe sources contribute to the total Fe budget of the central Pacific Ocean.

The large intra-epoch variation seen in past seawater $\delta^{56/54}$Fe necessitates that the dominant Fe sources to the Pacific have changed through time (Fig. 3). Assuming a fixed dust value of $\delta^{56/54}Fe \approx +0.7 \pm 0.1$ ‰ throughout the past 76 Myr, it is clear that more than 75 % of the record is outside of the field defined by mineral aerosol (Fig. 4). Isotopic mixing considerations[32] demand that Fe-isotopic values observed outside of this narrow range must originate from mixing with other Fe sources with different Fe-isotopic compositions (Fig. 3b).

Deep sources have been documented to possess $\delta^{56/54}$Fe that is highly variable and distinct from dust (Fig. 3a). Thus, the large range of Fe-isotopic compositions observed over the last 76 Myr require the addition of a quantitatively significant deeply sourced Fe pool to the central Pacific Ocean, such as sediment dissolution or hydrothermalism (Fig. 4). Applying a constant dust-derived $\delta^{56/54}Fe \approx +0.68 \pm 0.07$ ‰,[16] we note 12 distinct events where seawater Fe-isotopic compositions cross through the dust value (Fig. 4). To change seawater $\delta^{56/54}$Fe in the past from $< +0.61$ to > 0.75 ‰ (and vice versa) requires the input of an isotopically-distinct deep Fe source term to the central Pacific, as addition of more dust will simply drive the record towards +0.7 ‰. That these 'events' are not restricted to any particular epoch (though notably absent from the Pliocene onward), suggests deeply sourced Fe has been a significant and persistent component of the total Fe inventory of the Pacific Ocean throughout the past 76 Myr (Fig. 4).

Figure 4: Persistence of deeply sourced Fe in the Pacific Ocean. (*A*) Latitude of CD29-2 based on the migration of nearby DSDP locations.[60] (*B*) The Fe-isotopic history of central Pacific seawater recovered from Fe-Mn crust CD29-2 (squares). The high-resolution Fe-isotopic stratigraphy from 28DSR9[28] spanning the past $\sim$ 10 Ma is also shown, renormalized to IRMM-14 and corrected for $\Delta^{56/54}Fe_{FeMn-SW} = -0.77 \pm 0.06$ ‰ (triangles; 28DSR9 location shown in Fig. 1). Vertical arrows indicate the 12 instances where the Fe-isotopic composition of seawater transits the Fe-isotopic composition of dust (horizontal bar; ref.[16]) (*C*) Reconstructed Pacific Plate seafloor generation rate.[61] Both the spreading rate (mm yr^{-1}) and change in relative seafloor area (dA/dt, in km^2 100 yr^{-1}) are shown, as the total amount of new crust generated depends on total ridge length *and* spreading rate. (*D*) Records of eolian deposition in the N. Pacific ocean from DSDP 576[29] and LL44-GPC3;[30] note the logarithmic scale. The interrelationships between these three records is discussed in detail in the SI.

Understanding sustained changes in the Fe-isotopic composition of central Pacific seawater

The large intra-epoch variation in Fe-isotopic compositions recorded by CD29-2 necessitates a persistent influence of deep Fe sources to the total Fe inventory of Pacific seawater over the past 76 Myr. It is further possible to interpret some of the sustained excursions in $\delta^{56/54}$Fe (i.e. the inter-epoch variability) by understanding the location history CD29-2 and how this relates to probable changes in the supply rate of the major Fe sources to the ocean (Fig. 4). A detailed paleogeography of CD29-2 is discussed in Klemm *et al.*[59] Briefly, CD29-2 was situated at $\approx$ 6 °S at the time of its formation (76 Ma), crossed the equator around the K–Pg boundary ($\approx$ 66 Ma), and has gradually progressed to its present location at $\approx$ 16 °N (Fig. 4a). Thermal subsidence of the underlying oceanic lithosphere has likely increased the water depth from $\sim$ 1,000 to $\sim$ 2,000 m over the past 76 Myr, with the most rapid changes in depth occurring soon after CD29-2 began precipitating (see SI). With these considerations in mind, we discuss below the three most prominent features of the long term record: the excursion to extremely heavy $\delta^{56/54}$Fe during the Oligocene, the absence of large intra-epoch shifts after the Pliocene, and a possible shift to isotopically light values during the Upper Cretaceous (Fig. 4). The Oligocene data are discussed in detail in the SI, but are briefly summarized here.

The Oligocene data are best explained by a large and persistent increase in the hydrothermal contributions to the total Fe budget of water masses bathing CD29-2 during this epoch (Fig. 4). The extremely heavy $\delta^{56/54}$Fe of up to +2.3 ‰ necessitates that there were significant Fe-isotopic source modification processes that were able to deliver isotopically heavy Fe to the ocean without 'choking off' the Fe supply. Modification of hydrothermally-sourced Fe by precipitation of isotopically light Fe-sulfides seems an obvious candidate for such a process (e.g.;[52,57] SI). Hydrothermal vents can exude fluids with μM to mM Fe concentrations,[62] and the precipitation of Fe-sulfides from hydrothermal fluids – even at high temperatures – can result in significant Fe-isotopic modification of Fe fluxes (e.g.;[52] SI). Moreover, recent studies have documented distal transport of hydrothermally-sourced Fe thousands of kilometers across the Pacific that furthermore resemble the distributions of hydrothermally-derived helium anomalies (e.g[63,64]). Assuming that the modern correspondence between seafloor generation rate and hydrothermal fluid fluxes [REF?] was also valid in the past, it is tempting to speculate that this shift to heavy Fe-isotopic compositions in the Oligocene was driven by the approximate doubling of the rate of seafloor generation in the Pacific basin during this epoch (;[61] Fig. 4c). Conversely, CD29-2 was likely situated $\approx$ 11 °N during the Oligocene (Fig. 4a), which is now bathed by a distal 'jet' of hydrothermally-influenced deep waters between 1,500–3,000 m (evidenced by mantle-derived helium anomalies;[65]). Assuming that the vent systems at 9–10 °N along the EPR (East Pacific Rise) remained active during the Oligocene, and that the predominantly east-to-west geostrophic flow at these depths also persisted at this time,[66] it is conceivable that CD29-2 simply moved through a plume of hydrothermally influenced deep waters. Since there are no other elemental indications of hydrothermal influence on CD29-2 at this – or any other – time[19] during its $\approx$ 76 Myr growth history, the Fe-isotopic systematics of CD29-2 require an unprece-

dented degree of Fe-isotopic source modification to waters bathing CD29-2 during this epoch. However, testing whether or not this isotopically heavy reflects a basin wide increase in hydrothermally-derivd Fe during the Oligocene, or simply a local phenomenon will require a greater spatial resolution of Fe-Mn crust-derived records of seawater $\delta^{56/54}$Fe. Nonetheless, the remarkable degree of seawater Fe-isotopic variation across the Oligocene is encouraging, as it permits the testing and tracing of Fe-isotopic provinciality – and therefore Fe sources – in the ocean interior over geological time.

An important feature of the record is that the intra-epoch shifts in $\delta^{56/54}$Fe to values above and below the dust end-member appear to cease around the start of the Pliocene (arrows in Fig. 4). The large Fe-isotopic shifts seen throughout the rest of the record must be related to non dust-derived deep Fe sources such as hydrothermalism and marginal sediment dissolution. However, at some point during the past 10–20 Myr, the average Fe-isotopic composition of central Pacific seawater recorded by CD29-2 and 28DSR9 became largely invariant at $\delta^{56/54}\text{Fe} \approx +0.4 \pm 0.1$ ‰ ($\pm$2 SD). This switch to relative Fe-isotopic homogeneity over the past 10–20 Myr is consistent with a reduced importance of deeply sourced Fe and is coincident with the sharp increase in eolian dust deposition in the central and north Pacific (Fig. 4d;[29,30]). Since dust-derived Fe is thought to possess $\delta^{56/54}\text{Fe} \approx +0.7$ ‰,[16] the Fe-isotopic chemistry of CD29-2 is consistent with the interpretation that dust has provided a significant portion of the central Pacific Fe inventory from $\approx$ 10–20 Ma to the present day. However, the small difference between seawater ($\approx +0.4$ ‰; inferred from Fe-Mn crusts) and the dust end-member ($\approx +0.7$ ‰) of $\approx$ 0.3 ‰ is indicative of an influence from a secondary, isotopically light Fe source such as reductive sediment dissolution[67] or Fe-oxide-influenced hydrothermalism.[51]

The sustained shift to light Fe-isotopic ratios in the Upper Cretaceous are consistent with an increased influence of continental margin-sourced Fe, or hydrothermalism modified by Fe-oxide precipitation to waters bathing CD29-2. Reductive and non-reductive dissolution of sediments along continental margins contribute Fe to the ocean with light end-member Fe-isotopic compositions of $\delta^{56/54}\text{Fe} \sim -3$ ‰ and $\approx +0.2$ ‰, respectively (;[9,10] Fig. 3a). Analogous to Fe-sulfide modification processes described above, hydrothermal modification by Fe-oxide precipitation could also facilitate the release of isotopically light Fe to seawater.[16,51] Though it is currently not possible to distinguish between these two deep sources using $\delta^{56/54}$Fe, both of these probable sources possess substantially different Fe-isotopic fingerprints compared with surface dust deposition, thus ruling out a major atmospheric Fe contribution to seawater bathing CD29-2 during the Upper Cretaceous (Fig. 3). During the Upper Cretaceous, CD29-2 was likely at water depths $\approx$ 1,000 m (SI), and situated south of the equator at $\sim 6^{\circ}$S (;[59] Fig. 4a). This is somewhat above than most EPR-derived helium anomalies,[65] such that a shallower, marginal sedimentary Fe source is more likely. In the modern ocean, significant quantities of reduced,[68] bioavailable,[69] and isotopically light Fe[9,67] are released under low oxygen conditions associated with the highly productive western continental margins.[70] As such, the ≈ -0.3 ‰ shift to values ≈ 0 ‰ in Upper Cretaceous seawater $\delta^{56/54}$Fe recorded by CD29-2 are best explained by a greater importance of shelf sediment dissolution to the Fe budget of waters bathing CD29-2, further illustrating the power of $\delta^{56/54}$Fe to distinguish between surface and deep Fe sources through geological time.

Conclusions and outlook

The Fe-isotopic data for CD29-2 illustrate a dynamic Fe cycle in the central Pacific Ocean over the past 76 Myr. Isotopic mixing considerations demand a persistent and significant influence from deeply sourced Fe to the waters bathing CD29-2 in the central Pacific over the past 76 Myr. Deeply sourced Fe may have even contributed the majority of the Fe during certain epochs, such as during the Oligocene,

underscoring the importance of the oceans' circulation in controlling the spatial extent of deeply sourced Fe and its contribution to basin-scale Fe budgets. However, it is clear that more records of Fe-isotopic compositions from other Fe-Mn crusts are required to test the provinciality of oceanic Fe sources in the past; the long-term record from CD29-2 is merely the first step towards this goal.

Reconstructions of past oceanic Fe sources can reveal much about the oceans Fe cycle in the past, but it is clear that there is still much to learn. For example, what is the maximum lateral extent that dissolved $\delta^{56/54}$Fe signatures can persist across the ocean? Are there locations in the modern open ocean where dissolved $\delta^{56/54}$Fe exceeds +2 ‰? Did the deeply sourced Fe of the Oligocene ever ventilate at the surface? Is deeply sourced Fe an important contributor to the total Fe inventory in other ocean basins? Are the changes in the supply ratio of different Fe sources to the ocean responding to major climatic changes, or driving them? All of these questions can be tackled with a greater spatial coverage of dissolved $\delta^{56/54}$Fe in the modern ocean and by performing further paleoceanographic studies of past seawater $\delta^{56/54}$Fe in other ocean basins. Coupling these currently scant Fe-isotopic observations to models of global Fe biogeochemistry will help to iron-out these issues, and will refine our understanding of the role that different Fe sources play in modulating global climate.

Materials and Methods

The samples of CD29-2 analyzed in this study were previously collected for Tl- and Os-isotopic investigations, with discrete samples taken via microdrilling. The age model for the crust was determined by matching the Re decay-corrected Os-isotopic ratios for each discrete sample with the known osmium isotopic evolution of seawater. Sample aliquots were then purified for Fe-isotopic analysis using anion-exchange column chemistry and converted to nitrate form before mass spectrometric analysis. Iron isotopic analyses were carried out on a Nu Instruments Nu Plasma HR multiple-collector inductively coupled plasma mass spectrometer at the University of Oxford. Corrections for instrumental mass bias and isobaric overlap of ^{54}Cr on ^{54}Fe were performed by standard–sample bracketing and monitoring ^{53}Cr, respectively. Mass dependence, reproducibility, and accuracy were evaluated by analysis of various internal and external reference standards and found to be in excellent agreement with previously published values (where available). Further description of methods and samples is available in SI Materials and Methods.

ACKNOWLEDGMENTS. We thank D.N. Schmidt, T. van de Flierdt, T.M. Conway, W.B. Homoky, P.E. Lerner, J.D. Owens, S. Severmann, and – in particular – J.N. Fitzsimmons for some lively discussions; K.E. Egan and F. Poitrasson for constructive comments on an earlier version of this manuscript; and the editor and several anonymous reviewers for helping us to craft a substantially improved paper. T.J.H. is supported by the Postdoctoral Scholar Program at the Woods Hole Oceanographic Institution, with funding provided by the Doherty Foundation. H.M.W. is funded by the Natural Environment Research Council (Advanced Fellowship NE/F014295/1) and the European Research Council (Starting Grant 306655 'HabitablePlanet').

Supporting Information

SI Materials and Methods

Samples and sampling

Ferromanganese crust F7-86-HW CD29-2, referred to throughout the text as 'CD29-2', was recovered via dredging along the Karin Ridge, a submarine volcanic feature east of Johnston Island in the central Pacific.[20] Sample CD29-2 was recovered from the ridge flank at 16°42.4′ N; 168°14.2′ W, $\approx 200 - 600$ m from the ridge summit. The age of the base of the crust is $\approx$ 75.5 Ma,[23] based on an extrapolation of the average growth rate between the PETM ($\approx$ 55.5 Ma) and the Paleocene–Late Cretaceous boundary (66 Ma;[45]). Alkalic basalts from the ridge itself exhibit $^{40}Ar/^{39}Ar$ ages between $81.4 - 85.6$ Ma,[71] which are currently situated at 1,800 m depth. The flat top of the Karin Ridge is strong evidence that it was previously exposed above sea level,[72] implying that substantial thermal subsidence has occurred to the ridge over the past $81.4 - 85.6$ Myr, bathing CD29-2 in progressively deeper water masses. Assuming that this 1,800 m of subsidence occurred in proportion to $t^{\frac{1}{2}}$ (e.g. ref.[73]) over $\approx$ 83.5 Myr, CD29-2 likely formed in a water depth between $750 - 1,150$ m, and has subsided $\sim$ 16 m Myr^{-1} to its current depth between $1970 - 2390$ m. These water depth constraints, though necessarily rough, suggest that CD29-2 has been submerged below $\approx 1,000$ m for its entire growth history of $\approx$ 76 Myr.[23]

The samples analyzed in this study were previously collected for Tl- and Os-isotopic investigations,[23,74] where samples were drilled from slabs of CD29-2 at a spacing of 0.2, 0.5, or 1 mm via microdrilling. The age of the crust was determined by the osmium isotopic stratigraphy, where Re decay-corrected Os-isotopic ratios measured on discrete samples through the entire crust[74] were matched to the known Os-isotopic evolution of Cenozoic seawater (see[74] and references therein). Because portions of the Cenozoic Os-isotopic seawater curve are largely invariant, the age model for CD29-2 was constructed by identifying specific events characterized by large Os-isotopic excursions (such as the K–Pg and Eocene–Oligocene boundaries) and interpolating crust growth rates in between these fixed points. Therefore, absolute ages may be somewhat uncertain (up to several million years uncertainty) when furthest away from these fix points. However, the relative chronology of the crust is very robust as samples were drilled in sequence. The use of Os-isotopic stratigraphy to date Fe-Mn crusts is discussed in Klemm *et al.*,[74] and the revised age model used for CD29-2 is discussed in Nielsen *et al.*[23]

Analytical procedures

Powder samples of CD29-2 were leached in 6 M HCl, centrifuged, and transferred from 2 mL polypropylene centrifuge tubes into acid-cleaned Savillex vials and were evaporated to dryness and oxidized several times with hydrogen peroxide and concentrated nitric acid (Analar grade and Teflon-distilled, respectively) after which they were converted to chloride form via several reflux cycles with 6 M Teflon-distilled HCl. The samples were then purified for Fe using standard anion-exchange column chemistry,[75] and converted to nitrate form using hydrogen peroxide and concentrated nitric acid. The combined blank for sample dissolution and column chromatography was < 5 ng Fe; this is negligible relative to the amounts of Fe extracted from the samples (typically over 300 μg total Fe).

Iron isotopic analyses were carried out on the Nu Instruments Nu Plasma HR multiple-collector inductively coupled plasma mass spectrometer at the University of Oxford following established procedures.[76]

Samples were analyzed in 0.01 M HNO_3 and mass bias was corrected by sample–standard bracketing. Measurements included collection of ion currents on m/z: 57, 56, 54, and 53 (^{53}Cr), to allow for correction of any interference of ^{54}Cr on ^{54}Fe, although no difference between Cr-corrected and uncorrected ratios were observed; this is due to the purification of the samples prior to analysis and effective separation of Cr from Fe.

In order to monitor Fe-isotopic data quality and, in particular, the absence of artifacts relating to (i) incomplete Fe separation during column processing or (ii) sample matrix, several tests were performed. Firstly, aliquots of pure IRMM-14 Fe standard (by definition, $\delta^{56/54}$Fe of IRMM-14 $\equiv$ 0 ‰) were passed through columns. Column-processed IRMM-14 yielded $\delta^{56/54}\text{Fe} = 0.00 \pm 0.06$ ‰ (2 SD, $n = 3$) with a recovery of 100 ± 2 %, demonstrating that no Fe-isotopic fractionation took place during column processing and that Fe yields were quantitative, respectively. Secondly, sample matrix effects were evaluated by performing IRMM-doped sample matrix tests. All Fe-free sample matrix fractions were retained during column chromatography, and those corresponding to CD29-2 33.2 mm and 34.2 mm (Table 2) were doped with IRMM-14 to match the original Fe : matrix ratio of the corresponding sample. These IRMM-14-doped samples of CD29-2 were then re-processed through column chromatography and analyzed for their Fe-isotopic compositions, yielding $\delta^{56/54}\text{Fe} = +0.01 \pm 0.07$ ‰ (2 SD, $n = 3$) and -0.03 ± 0.09 ‰ (2 SD, $n = 2$) for CD29-2 33.2 mm and 34.2 mm, respectively.

Reproducibility and accuracy were also evaluated by analysis of several in-house and international Fe-isotopic reference standards:

- An in-house FeCl powder, obtained from the ETH Zürich (ETH Fe salt standard); $\delta^{56/54}\text{Fe} = -0.73 \pm 0.10$ ‰ (2 SD, $n = 48$), in agreement with published values from Mikutta *et al.*[77] of $\delta^{56/54}\text{Fe} = -0.72 \pm 0.13$ ‰.
- USGS Pacific Fe-Mn nodule sample (Nod-P-1); $\delta^{56/54}\text{Fe} = -0.39 \pm 0.07$ ‰ (2 SD, $n = 7$), in agreement with published values from Dideriksen *et al.*:[78] $\delta^{56/54}\text{Fe} = -0.42 \pm 0.09$ ‰.
- USGS Icelandic Basalt sample (BIR-1); $\delta^{56/54}\text{Fe} = +0.04 \pm 0.07$ ‰ (2 SD, $n = 4$), in excellent agreement with published values from Weyer *et al.*:[79] $\delta^{56/54}\text{Fe} = +0.05 \pm 0.04$ ‰.

SI Discussion

Estimating Fe diffusivity in Fe-Mn crusts

Diffusional resetting or 'smoothing' of primary signals can affect certain trace metal isotopic records recovered from Fe-Mn crusts (e.g.[26,80]). To assess if this was an issue for records of Fe-isotopic compositions recorded by CD29-2, we estimated the diffusivity of Fe in Fe-Mn crusts by assuming that the rate of chemical exchange between fluid (seawater) and solid (Fe-Mn crusts) is governed by the same processes for Fe as for U. From this, we applied the general Fe-Mn crust diffusivity equation from Henderson and Burton:[26]

$$D_{\text{eff.}}^{\text{Fe}} = \frac{D_{\text{eff.}}^{\text{U}} K_{\text{c}}^{\text{U}}}{K_{\text{c}}^{\text{Fe}}} \tag{1}$$

Figure 5: The ancient biological origin of siderophore production. Percent identity of BLASTp results from (*A*) enterobactin synthase subunit F (EntF) and (*B*) desferrioxamine E biosynthesis protein DesA. All sequences have been ordered by e-value (low to high), showing percent identities for sequences with e-values <1E-5 and <2E-30 for EntF and DesA, respectively (mean DesA sequence length is 419 amino acids).

where $D^{E}_{eff.}$ is the effective diffusivity of element E in Fe-Mn crusts ($cm^2\ yr^{-1}$) and K^{E}_{c} is the concentration ratio of E in Fe-Mn crusts relative to its porewaters (assumed to be seawater;[26]). Assuming a range of [Fe] for deep Pacific seawater between $0.4 - 0.6$ nM[81] and [Fe] of CD29-2 crusts between $10 - 20$ wt. %,[19] the Fe concentration ratio between CD29-2 : seawater is between $3 - 9 \times 10^9$. As such, we calculate $D^{Fe}_{eff.}$ between 4×10^{-13} and 1×10^{-12} $cm^2\ yr^{-1}$. Such a slow rate of Fe diffusion – at least half the rate of Th diffusivity in Fe-Mn crusts[26] – suggests that our Fe-isotopic dataset is a primary record and has not been smoothed or reset by diffusion. Diagenetic precipitation of calcium fluorapatite (calcium fluorophosphate) in the lower half of CD29-2 (e.g.[19,27]) does not appear to affect $\delta^{56/54}$Fe. This is likely because secondary calcium fluorapatite contains little, if any, Fe compared to the average 15 wt. % Fe of CD29-2, and the predominantly pore-filling nature of calcium fluorapatite precipitation that primarily serves to reduce Fe-Mn crust porosity.

The age and origin of strong Fe-binding ligands in the ocean

While neither the composition of the strong ligands in ocean seawater nor microbial siderophore biosynthetic pathways specific to abundant marine microbes are known, the global prevalence of seawater Fe ligands and the similarity of their similar conditional binding strengths to those of siderophores strongly implies a contribution of siderophores to the oceanic Fe ligand inventory.[44] Moreover, field studies have identified ferrioxamine-type ligands in seawater enrichment studies,[43] demonstrating the presence of siderophore biosynthetic capacity in natural assemblages and bolstering the case for their contribution to the oceanic Fe ligand reservoir.

Two types of biosynthetic pathways for siderophores are currently known, non-ribosomal peptide synthesis (NRPS) and NRPS-independent siderophore synthesis (NIS).[82] To examine if siderophore synthesis is older than the $\approx$ 76 Myr time period of interest in this study, we examined the diversity of a gene across numerous microbial genomes from each of these two siderophore biosynthetic pathways, focusing on the specific siderophores desferrioxamine E biosynthesis protein DesA and enterobactin synthase subunit F (EntF). EntF is a component of a three protein NRPS complex,[83,84] and DesA was recently implicated in NIS siderophore synthesis.[82] Microbial genomes were analyzed using the Standard Protein Basic Local Alignment Search Tool (BLASTp;[85]), which is used to identify seed amino acid sequences (the query) in other organisms by searching within a specified database. For each query, regions of similarity (identity) and their alignment with other amino acid sequences are identified. Each potential match is scored and assigned an e-value (expected value), which decreases exponentially towards 0 the higher the statistical confidence that the match is not simply chance. Using BLASTp and the non-redundant sequence database with seed sequences from siderophore-producing model bacteria (*E. coli* and *Streptomyces sp.*), sequence search and alignments showed each gene to correspond to a broad range of sequence identities across diverse range of microbes, extending to as low as $\approx$ 30 % identity while maintaining low e-values consistent with a shared ancestral origin (Fig. 5; Tables 3 and 4).

Amino acid sequence alignments and identities have been used to attempt to calculate evolutionary distance and divergence times of major taxa throughout Earth history, using a calibration against the

vertebrate fossil record.[86,87] Using a conservative approach here, a comparison of the range of sequence identities from the two siderophore biosynthetic gene identities with the previous approaches to constrain the age of divergence major groups of organisms using amino acid distance measurements, implies that the last common ancestor for both genes is extremely old. For example, the evolutionary distances that corresponds to a 91 % identity is estimated to have a last common ancestor (divergence) of 100 Ma, whilst a 60 % identity corresponds to more than 1,000 Ma.[88] Both of these estimates are higher in identity than the homologous sequences examined here, hence implying these biosynthetic genes diverged from a last common ancestor far longer than the $\approx$ 76 Myr timescale of this study (Tables 3 and 4). This observation remains true even if with the caveat that the calculated ages for bacterial sequences may be biased several-fold faster due to a distinct synonymous substitution rate in bacteria relative to the calibrated vertebrate fossil record.[89]

As expected, sequences with higher percentage identities are found within the same species (e.g. *E. coli* for EntF) and hence most likely share siderophore biosynthetic function. Yet at lower identities it can be more challenging to constrain protein function due to limited experimental evidence and potential recruitment from related enzyme pathways. In the case of the enterobactin EntF gene, *Salmonella sp.* are known to also produce enterobactin using this pathway,[90] providing support for this siderophore biosynthetic function. EntF of Salmonella sp. has a $\approx$ 80 % sequence identity, implying an age of over 300 Ma for a divergence from a shared genetic ancestor using the approach described above (Table 3). Other sequences within the lower range of sequence identity are annotated as EntF and may have similar siderophore biosynthesis function. For DesA, annotations of homologous sequences correspond to DesA or the enzyme L-2,4-diaminobutyrate aminotransferase. Recent biochemical and genomic characterization of this enzyme have demonstrated it to have the lysine carboxylase activity required as a key step in NIS siderophore biosynthesis and to be broadly disseminated in bacteria,[82] consistent with the search results in Table 4.

Together, these calculated evolutionary distances for two gene representatives of two siderophore biosynthetic pathways show them both to be much older than the $\approx$ 76 Myr time span focused on in this study. Overall, these observations lend support to the notion that the siderophore biosynthetic pathways that may contribute seawater Fe ligand production are similarly old and that the resulting ligand-mediated Fe-isotopic offsets in seawater – $\Delta^{56/54}Fe_{\text{dust part.}-\text{dust diss.}}$ and $\Delta^{56/54}Fe_{\text{FeMn}-\text{SW}}$) – have also been stable for $\approx$ 76 My, if not far longer.

Deeply sourced Fe persists regardless of how the dust value is assigned

The interpretation that deeply sourced Fe has been important in the Pacific Ocean for the past 76 Myr is robust regardless of how the dust-derived Fe-isotopic end-member is assigned. If dust-derived $\delta^{56/54}$Fe was not $+0.7 \pm 0.1$ ‰ but possessed a different value, there is no unique Fe-isotopic composition of dust-derived Fe that can account for the entire record without requiring mixing with another deep Fe source that has a distinct Fe-isotopic composition; such a scenario is only possible if $\Delta^{56/54}Fe_{\text{FeMn}-\text{SW}}$ also changed. However, temporally-constant seawater $\delta^{56/54}$Fe with temporally variable $\Delta^{56/54}Fe_{\text{FeMn}-\text{SW}}$ is essentially precluded by the following considerations. Firstly, for seawater $\delta^{56/54}$Fe to have remained constant, $\delta^{56/54}$Fe heavier than $\approx$ +0.5 ‰ recorded by CD29-2 would necessitate periodic reversals in the sense of Fe-isotopic fractionation between Fe-Mn crusts and seawater. Given the mineralogical homogeneity of CD29-2,[19] we consider such a scenario highly implausible. Secondly, there is no evidence to suggest that $\Delta^{56/54}Fe_{\text{FeMn}-\text{SW}}$ is variable in the modern ocean, despite the large range of depths, [Fe], and $\delta^{56/54}$Fe encountered in the offset calibration ($\sim 200 - 4,000$ m, $\approx 0.4 - 1$ nM, $\approx +0.2$ to $+0.7$ ‰,

Figure 6: Pb-isotopic array for CD29-2. Plot of $^{207}Pb/^{206}Pb$ vs. $^{208}Pb/^{206}Pb$ for CD29-2 from Christensen *et al.*[91] using the age model of Nielsen *et al.*[23] Given that the Pb-isotopic data were not obtained on the same slab of CD29-2 as the Os-isotopic stratigraphy, the absolute ages for the Pb-isotopic data have considerable uncertainty. To account for this uncertainty, the Pb-isotopic data have not been re-plotted against age, but instead have been binned into their respective geological Epochs to illustrate broad temporal patterns. Pb-isotopic uncertainties are shown at the 2 SD level and are discussed in Christensen *et al.*[91]

respectively; Fig. 2; Table 1). Thirdly, current evidence suggests that Fe-isotopic offsets between Fe-oxides and ligand-stabilized dissolved Fe(III), and by analogy $\Delta^{56/54}Fe_{FeMn-SW}$, is primarily governed by ligands,[53] which have an ancient biological origin and are thus likely present throughout the 76 Myr record sampled by CD29-2 (SI Discussion). Whilst it is not possible to definitively demonstrate that $\Delta^{56/54}Fe_{FeMn-SW}$ did not change in the past, all available evidence supports the use of a temporally-constant $\Delta^{56/54}Fe_{FeMn-SW}$ of -0.77 ± 0.06 ‰ for the past 76 Myr.

What drove the excursion to extremely heavy Fe-isotopic compositions during the Oligocene?

The processes that may have affected the Fe-isotopic composition of central Pacific seawater over the past 76 Myr can be broadly subdivided into two categories based on their overall mechanism of influencing seawater Fe-isotopic chemistry: indirect and direct influences. Indirect influences on seawater Fe-isotopic chemistry are those processes that affect the cycling of Fe within the ocean interior, but do not necessarily alter the marine Fe inventory. Direct influences are those processes that alter the oceanic inventory of Fe and/or the Fe-isotopic modification of a source as it becomes stabilized in seawater. There is considerable evidence to suggest that direct factors exert the primary control on modern oceanic $\delta^{56/54}Fe$, such as the large range of Fe-isotopic compositions measured between the principal marine Fe sources (Fig. 3a) and the numerous documented Fe-isotopic source modification processes that can supply isotopically fractionated Fe to the oceans (e.g.,[10,52,55,57] Fig. 3a). We briefly outline how indirect influences are unlikely to be a major control on seawater $\delta^{56/54}Fe$, before discussing each of the major features of the Fe-isotopic record in the text below.

The most important of the indirect influences on central Pacific seawater Fe-isotopic compositions are likely to be changes in deep water circulation patterns over the past 76 Myr. Though changes in the depth of carbonate compensation[92] and changes in atmospheric pCO_2[93] have occurred during the record, it is not clear how these processes would affect seawater $\delta^{56/54}Fe$. However, changes in deep water circulation would result in CD29-2 being bathed in different water masses throughout its growth, which would cause $\delta^{56/54}Fe$ to vary so long as different water masses possessed distinct Fe-isotopic compositions. Since little is known about Pacific deep water mass geometry throughout the Cenozoic, it is only possible to infer changes in ambient water masses through comparison with other geochemical proxy records recovered from CD29-2. The high-resolution Pb-isotopic stratigraphy of Christensen *et al.*[91] would appear to support this inference, as the Pb-isotopic data for CD29-2 indicate numerous changes in central Pacific Pb sources over the Cenozoic (Fig. 6). However, the three main Pb-isotopic arrays[91] do not correspond to major features of the Fe-isotopic record (Fig. 3b), and it is unclear if the Pb- and Fe-isotopic records from CD29-2 are directly comparable given the differing geochemical behaviors of these two elements in seawater (e.g.[25]). Ultimately a water mass structure control on central Pacific $\delta^{56/54}Fe$ still implies that distinct Fe sources (i.e. direct factors) exert the dominant control over seawater $\delta^{56/54}Fe$, but that indirect factors determine the Fe-isotopic depth structure of the water column. With this in mind, we interpret the major shifts in the seawater Fe-isotopic record from CD29-2 in terms of changes in the relative balance and/or modifications to the dominant Fe fluxes to the ocean through time.

The Fe-isotopic record indicates that central Pacific seawater was as heavy as $\delta^{56/54}$Fe $\approx +2.3$ ‰ during the Oligocene, with a sustained shift to values $\approx +0.8$ ‰ heavier than the mean value of the other epochs (Fig. 4). The Oligocene is notable for numerous environmental changes, including: a drop in global sea-level and the emplacement of major ice sheets on Antarctica, a global increase in chemical weathering rates, a deepening of the carbonate compensation depth, a drop in atmospheric pCO_2, a significant increase in seafloor generation rate in the Pacific basin, and the opening of the Antarctic seaways (e.g.[61,91–94]). We outline below why an increased rate of seafloor generation and associated hydrothermal fluid fluxes in the Oligocene is likely responsible for the observed shift in seawater $\delta^{56/54}$Fe, although we concede that it is difficult to entirely rule out other possible explanations for the Oligocene data.

In the modern ocean, isotopically-heavy Fe sources share an important characteristic: modification by Fe-sulfide precipitation. A shift to heavier Fe-isotopic compositions is thus inconsistent with an increased Fe flux from reductive sediment dissolution (~ -3 ‰;[9] Fig. 3a) or increased source modification by Fe-oxide precipitation, as both of these factors would drive marine Fe-isotopic compositions toward lighter values. The sustained shift to isotopically heavy $\delta^{56/54}$Fe in the Oligocene must relate to increased source modification by Fe-sulfide precipitation (Fig. 4), as this is the only plausible modification process that can generate heavy Fe-isotopic compositions. Fe-sulfide precipitation can occur in continental margin[10,55] and hydrothermal settings,[57] and has been documented to drive residual, dissolved Fe towards heavy $\delta^{56/54}$Fe in field settings. In sedimentary systems with oxic bottom waters, Fe-sulfide precipitation (usually as pyrite[56]) occurs well below the sediment–water interface in sulfidic sedimentary horizons.[10,55] These sulfidic redox horizons are frequently characterized by low ambient [Fe], as abundant free sulfide will favor the precipitation of Fe-sulfide minerals, thus 'choking off' the benthic Fe supply. Overall, these considerations suggest that the Fe-sulfide-influenced Fe flux from continental margins is unlikely to have a significant influence on open ocean $\delta^{56/54}$Fe.

Precipitation of Fe-sulfide also occurs in deep-sea hydrothermal systems, which account for large fluxes of Fe to the deep ocean[6,8,63,95,96] that can be stabilized by organic compounds.[48] End-member hydrothermal fluids appear to possess $\delta^{56/54}$Fe ≈ -0.2 ‰ (Fig. 3a;[51,52]), although ligand-stabilized Fe that escapes the local hydrothermal source may be significantly modified toward heavier or lighter $\delta^{56/54}$Fe, depending on the proportion of Fe-oxide versus Fe-sulfide precipitation ($\Delta^{56/54}\text{Fe}_{\text{oxide}-\text{dissolved}} > 0$; $\Delta^{56/54}\text{Fe}_{\text{sulfide}-\text{dissolved}} < 0$). The partitioning of Fe between oxides and sulfides depends primarily on the Fe : H_2S ratio of the vent fluids and the kinetics of Fe(II) oxidation in ambient seawater.[51] In the high (> 20;[51]) Fe : H_2S ultramafic-hosted Rainbow hydrothermal system in the north Atlantic, Fe precipitation is near-quantitative and occurs almost exclusively as Fe-oxides that exhibit Fe-isotopic compositions similar to end-member hydrothermal fluid.[51] In other basalt-hosted Atlantic vent systems, where Fe : H_2S is ~ 1,[97] significant Fe-isotopic fractionation has been observed, resulting in a net transfer of isotopically heavy dissolved Fe to seawater.[57] The hydrothermal systems of the EPR (East Pacific Rise) exhibit even lower Fe : H_2S ratios ≤ 0.1,[98] such that dissolved Fe escaping to seawater is expected to exhibit extremely heavy Fe-isotopic compositions. Unpublished Fe-isotopic profiles of seawater from the southeast Pacific Ocean appear to confirm this phenomenon,[99] though open ocean seawater values in excess of $\delta^{56/54}$Fe $\sim +1$ ‰ remain to be observed.

Indirect evidence for an important role for hydrothermal Fe-sulfide precipitation can be obtained via examination of the Fe-rich hydrothermal precipitates at active vent sites (i.e. the reaction products of the Fe source modification processes). Fe-isotopic analyses of pyrite-rich hydrothermal chimneys from the EPR exhibit $\delta^{56/54}$Fe between ≈ -1.3 and -0.5 ‰, thus requiring the accompanying 350 °C hydrothermal fluids to possess $\delta^{56/54}$Fe between $+1.0$ and $+1.5$ ‰ (at equilibrium;[52]). Even heavier Fe-isotopic compositions are theoretically possible if Fe-isotopic fractionation follows a Rayleigh distillation inside

the hydrothermal stockwork. For example, in a hydrothermal system with ≈ 97 % precipitation of an initial hydrothermal fluid characterized by $\delta^{56/54}\text{Fe} = -0.2$ ‰,[51] the residual dissolved $\delta^{56/54}\text{Fe}$ should be in excess of +2 ‰ assuming all precipitation as Fe-sulfides when $\Delta^{56/54}\text{Fe}_{\text{sulfide-dissolved}} = -0.6$ ‰[57]. At 99 % precipitation, residual $\delta^{56/54}\text{Fe}$ would reach ≈ +3 ‰, suggesting that the cumulative Fe-isotopic composition of precipitates formed from that system would exhibit $\delta^{56/54}\text{Fe} \approx -0.2$ ‰. Indeed, pyrite-rich hydrothermal precipitates at certain EPR vent sites have been shown to exhibit $\delta^{56/54}\text{Fe} \approx -0.2$ ‰ in field settings.[52] The Fe-isotopic values observed in the Oligocene strongly indicate that deeply sourced hydrothermal Fe dominated the total Fe inventory of the central Pacific, and that Fe-sulfide precipitation was the major source modification process at that time.

The Oligocene shift to heavy seawater $\delta^{56/54}\text{Fe}$ is coincident with a time of increased seafloor generation rate (assumed to be a proxy for hydrothermal activity;[61] Fig. 4c) in the Pacific basin and extremely low rates of eolian deposition (Fig. 4d). The confluence of these two factors likely explains the sustained shift to heavy values during this epoch. During the Oligocene, CD29-2 was situated at an average latitude of 11 °N, which would place it at the periphery of the maximum modern primordial $\delta(^3\text{He})$ anomaly in the central Pacific at $\sim 2,000$ m.[65] (Primordial $\delta(^3\text{He})$ anomalies are sourced through the degassing of mantle-derived ^{3}He at hydrothermal vents.[100]) The extremely low dust fluxes of the Oligocene (;[29,30] Fig. 4d) would have provided little Fe to buffer against this predominantly hydrothermally-sourced Fe anomaly. Though hydrothermal fluxes are also relatively high in the modern Pacific ocean compared to the rest of the Cenozoic,[61] the $\delta^{56/54}\text{Fe}$ of seawater ambient to CD29-2 has been lighter than either the Oligocene values or dust value since the Pliocene (Fig. 3b). The reduced influence of deeply sourced Fe on modern central Pacific $\delta^{56/54}\text{Fe}$ may reflect the significant increase in eolian-sourced Fe since the mid-Pliocene, the transit of CD29-2 to more northerly latitudes away from the primordial $\delta(^3\text{He})$ anomaly, or a change in the chemistry of EPR vent fluids since the Oligocene.

Deeply-derived hydrothermal Fe is increasingly recognized as an important component of the total Fe inventory of the modern deep Pacific,[6,63,64] as well as other ocean basins (e.g.[8,101–103]). Our Fe-isotopic record from CD29-2 suggests that this has also been true in the past, and that deeply sourced hydrothermal Fe was likely the major Fe source to water masses bathing CD29-2 during the Oligocene. More broadly, these data underscore the fact that multiple Fe sources contribute to the deep oceans' Fe inventory, and illustrate that the relative importance of these sources – and their Fe-isotopic chemistry – have also varied significantly through time.

Data Tables

Table 1: Fe-Mn crust–seawater data pairs used to calculate $\Delta^{56/54}Fe_{FeMn-SW}$. Fe-Mn crust data from Levasseur *et al.*;[33] seawater Fe-isotopic data from Conway & John.[16] Linear interpolation was used to estimated [Fe] and $\delta^{56/54}$Fe for seawater samples; uncertainties are as reported in the original publications.

Cruise	Sample	Distance (km)	Depth to σ_θ (m)	Interp. [Fe] (nM)	Interp. $\delta^{56/54}$Fe SW	±2 SD	$\Delta^{56/54}Fe_{FeMn-SW}$	±2 SD
ALV539	D2-1A	657	2423	0.61	0.53	0.05	-0.77	0.06
		681	2249	0.66	0.59	0.07	-0.83	0.07
		702	2686	0.67	0.51	0.06	-0.75	0.07
SO-154	52 CD-1	1552	863	0.53	0.52	0.07	-0.71	0.08
		1685	897	0.68	0.24	0.05	-0.43	0.07
		1782	727	0.46	0.54	0.07	-0.73	0.08
Arcl TR079	D14	1484	2074	0.63	0.60	0.08	-0.78	0.10
		1671	2294	0.61	0.56	0.06	-0.74	0.09
		1674	1900	0.66	0.59	0.06	-0.77	0.09
Gosnold 65-75	2383.00	1144	376	0.64	0.21	0.05	-0.78	0.10
		1171	243	0.39	0.55	0.09	-1.12	0.13
		1190	190	0.69	0.30	0.06	-0.87	0.11
	BM1963.897	1189	646	0.74	0.27	0.04	-0.52	0.09
		1224	393	0.43	0.51	0.09	-0.75	0.12
		1226	900	0.66	0.19	0.06	-0.44	0.10
Hudson St. 54	BM1969.05	635	1891	0.71	0.36	0.05	-0.84	0.11
		675	1761	0.68	0.44	0.05	-0.92	0.11
		707	1643	0.81	0.18	0.05	-0.67	0.11
Discovery 144	D10979	1541	4000	0.46	0.74	0.11	-1.02	0.11
		1603	3500	0.47	0.70	0.07	-0.98	0.08
		1684	3500	0.59	0.61	0.06	-0.89	0.08
VEMA CH 78	DR01-001a	1490	3217	0.48	0.71	0.07	-0.86	0.09
		1524	3771	0.50	0.60	0.06	-0.75	0.08
		1733	3317	0.49	0.74	0.08	-0.90	0.10
Atlantis II 96	D10-7	438	2488	0.47	0.70	0.06	-0.75	0.08
		677	2460	0.97	0.39	0.04	-0.44	0.06
		895	1984	0.54	0.67	0.06	-0.72	0.07
						Mean value ±2 SE	**-0.77**	**0.06**

Table 2: Fe-isotopic record from central Pacific Fe-Mn crust CD29-2. See text in Methods for age model description.
[a]Depth from top in mm
[b]Fractional depth in the crust
[c]Model age from[23]
[d]Surface value from[33]

DfT[a]	$\delta^{56/54}$Fe	±2 SD	f^b	Age[c] (Ma)	DfT[a]	$\delta^{56/54}$Fe	±2 SD	f^b	Age[c] (Ma)
0.5	−0.41[d]	0.09	0.0047	0.27	43.2	+0.01	0.08	0.4075	42.26
16.5	−0.25	0.09	0.1557	8.85	57.0	+0.71	0.06	0.5377	47.44
20.5	−0.07	0.04	0.1934	11.00	60.0	+0.27	0.10	0.5660	48.56
28.5	−0.25	0.09	0.2689	22.06	65.0	+0.11	0.10	0.6132	50.44
29.0	+0.39	0.08	0.2736	22.75	67.0	+0.40	0.02	0.6321	51.19
30.0	+1.21	0.03	0.2830	24.13	69.0	−0.02	0.02	0.6509	51.94
30.5	+0.28	0.13	0.2877	24.82	69.5	−0.05	0.03	0.6557	52.13
31.5	+0.08	0.10	0.2972	26.20	70.0	+0.15	0.04	0.6604	52.31
32.5	+1.54	0.08	0.3066	27.59	70.5	+0.06	0.05	0.6651	52.50
33.2	+0.79	0.07	0.3132	28.55	71.0	+0.13	0.04	0.6698	52.69
34.2	+1.31	0.09	0.3226	29.94	71.5	−0.38	0.06	0.6745	52.88
35.2	+1.32	0.02	0.3321	31.32	73.0	−0.90	0.06	0.6887	53.44
35.4	+0.62	0.06	0.3340	31.59	73.5	−0.13	0.02	0.6934	53.63
35.6	−0.69	0.05	0.3358	31.87	74.0	−1.12	0.10	0.6981	53.81
37.0	+0.06	0.05	0.3491	33.81	75.0	−0.17	0.08	0.7075	54.19
37.2	−0.01	0.10	0.3509	34.08	80.0	−0.03	0.07	0.7547	56.70
37.8	−0.57	0.10	0.3566	34.65	83.0	−0.06	0.05	0.7830	59.10
40.0	−0.11	0.01	0.3774	35.75	86.5	+0.02	0.11	0.8160	61.90
40.4	+0.21	0.10	0.3811	35.95	90.5	+0.35	0.07	0.8538	65.10
40.6	+0.03	0.10	0.3830	36.05	91.0	−0.25	0.09	0.8585	65.50
40.8	−0.04	0.19	0.3849	36.15	91.5	−0.83	0.12	0.8632	65.90
41.0	−0.11	0.02	0.3868	36.25	93.5	−0.75	0.14	0.8821	67.50
41.2	−0.07	0.02	0.3887	36.35	95.5	−0.69	0.06	0.9009	69.10
41.4	−0.02	0.05	0.3906	36.45	96.0	−0.28	0.06	0.9057	69.50
41.6	−0.67	0.08	0.3925	36.55	97.0	−0.78	0.12	0.9151	70.30
41.8	−0.08	0.05	0.3943	36.65	100.0	−0.60	0.10	0.9434	72.69
42.0	−0.47	0.10	0.3962	36.75	102.0	−0.43	0.02	0.9623	74.29
42.4	−0.03	0.03	0.4000	36.95	102.5	+0.17	0.05	0.9670	74.69
42.6	−0.03	0.09	0.4019	42.04	104.0	−0.30	0.09	0.9811	75.89

Table 3: Selected search results from BLASTp output of enterobactin synthase subunit F against non-redundant sequence database (NR). Many homologous proteins are detected within existing the current sequence databases, extending to sequences with amino acid identities as low as $\approx$ 30 %, with many of these being annotated as being related to enterobactin biosynthesis, and others being related to the larger non-ribosomal peptide synthesis group to which this enzyme belongs.

E-value	% identity	Taxon	BLASTp Annotation	Taxon Group
0	100.00	*Escherichia coli;Escherichia coli* K-12	enterobactin synthase multienzyme complex component	enterobacteria
0	98.53	*Escherichia coli; Escherichia coli* ATCC 8739	enterobactin synthase subunit F	enterobacteria
0	81.98	*Shigella flexneri* 1235-66	enterobactin synthase component F	enterobacteria
0	81.67	*Citrobacter rodentium;Citrobacter rodentium* ICC168	enterobactin synthetase component F	enterobacteria
0	79.21	*Salmonella enterica; Oranienburg* str. 0250	enterobactin synthase subunit F	enterobacteria
0	78.13	*Klebsiella pneumoniae;Klebsiella pneumoniae* UHKPC06	enterobactin synthetase component F	enterobacteria
0	78.13	*Hafnia alvei* BIDMC 31	enterobactin synthase component F	enterobacteria
0	76.89	*Kosakonia radicincitans;Enterobacter radicincitans* DSM 16656	enterobactin synthase subunit F	enterobacteria
0	58.37	gamma proteobacterium WG36	enterobactin synthase subunit F	g-proteobacteria
0	58.31	*Pseudomonas sp.* 313	enterobactin synthase subunit F	g-proteobacteria
0	49.57	*Methylocystis rosea*	hypothetical protein	a-proteobacteria
0	44.26	*Marinomonas sp.* D104	chromophore lyase	g-proteobacteria
0	42.74	*Marinomonas mediterranea* MMB-1	amino acid adenylation protein	g-proteobacteria
0	40.39	*Vibrio campbellii*	peptide synthetase	g-proteobacteria
0	37.75	*Stenotrophomonas maltophilia* 5BA-I-2	enterobactin synthase	g-proteobacteria
0	36.96	*Aeromonas veronii; Aeromonas veronii* AER39	enterobactin synthase	g-proteobacteria
2.E-173	34.75	*Bacillus amyloliquefaciens;Bacillus amyloliquefaciens* DSM 7	siderophore 2	firmicutes
8.E-139	33.83	*Actinokineospora sp.* EG49	Siderophore biosynthesis non-ribosomal peptide synthetase module	high GC Gram+
2.E-127	32.41	*Methylobacter marinus*	hypothetical protein	g-proteobacteria
6.E-164	31.13	*Cyanothece sp.* PCC 7424	amino acid adenylation protein	cyanobacteria
1.E-88	29.18	*Rhodococcus opacus;Rhodococcus opacus* M213	non-ribosomal peptide synthetase	high GC Gram+

Table 4: Selected search results from BLASTp output of desferrioxamine E biosynthesis protein DesA against non-redundant sequence database (NR). Many homologous proteins are detected within existing the current sequence databases, extending to sequences with amino acid identities as low as $\approx$ 30 %, although most annotations are related to carboxylase or hypothetical proteins.

E-value	% identity	Taxon	BLASTp Annotation	Taxon Group
0	100.00	*Streptomyces sp.* PAMC26508	desferrioxamine E biosynthesis protein DesA @ Siderophore biosynthesis L-2	high GC Gram+
0	99.38	*Streptomyces flavogriseus* ATCC 33331	pyridoxal-dependent decarboxylase	high GC Gram+
0	85.03	*Streptomyces globisporus*	pyridoxal-dependent decarboxylase	high GC Gram+
0	82.50	*Streptomyces scabiei* 87.22	siderophore biosynthesis pyridoxal-dependent decarboxylase DesA	high GC Gram+
0	82.46	*Streptomyces sp.* CNS615	pyridoxal-dependent decarboxylase	high GC Gram+
0	77.96	*Streptomyces albus* J1074	4-diaminobutyrate decarboxylase, pyridoxal-dependent decarboxylase	high GC Gram+
0	70.23	*Streptomyces sp.* FxanaC1	pyridoxal-dependent decarboxylase	high GC Gram+
0	65.42	*Salinispora pacifica*	pyridoxal-dependent decarboxylase	high GC Gram+
0	64.07	*Actinopolyspora halophila*	hypothetical protein	high GC Gram+
0	62.91	*Nocardiopsis halotolerans*	pyridoxal-dependent decarboxylase	high GC Gram+
0	59.34	*Pseudomonas stutzeri* B1SMN1	tyrosine decarboxylase	g-proteobacteria
0	58.23	*Pseudomonas sp.* HPB0071	hypothetical protein	g-proteobacteria
0	57.71	*Pantoea agglomerans* 299R	Desferrioxamine E biosynthesis protein DesA	enterobacteria
0	56.82	*Marinobacterium rhizophilum*	hypothetical protein	g-proteobacteria
0	55.78	*Methylobacter marinus*	hypothetical protein	g-proteobacteria
5.E-168	50.10	*Pseudoalteromonas tunicata* D2	cytochrome C biogenesis protein CcmH	g-proteobacteria
7.E-114	44.61	*Halalkalicoccus jeotgali* B3	4-diaminobutyrate decarboxylase, Pyridoxal-dependent decarboxylase	euryarchaeotes
3.E-108	39.71	*Vibrio fluvialis* PG41	Diaminobutyrate–2-oxoglutarate aminotransferase	g-proteobacteria
2.E-47	36.39	*Synechococcus elongatus* PCC 6301	L-2-diaminobutyrate decarboxylase	cyanobacteria

References

[1] Twining BS, Baines SB (2013) The Trace Metal Composition of Marine Phytoplankton. *Ann. Rev. Mar. Sci.* 5:191–215.

[2] Boyd PW, et al. (2007) Mesoscale iron enrichment experiments 1993-2005: Synthesis and future directions. *Science* 315:612–617.

[3] Aumont O, Maier-Reimer E, Blain S, Monfray P (2003) An ecosystem model of the global ocean including Fe, Si, P colimitations. *Global Biogeochem. Cycles* 17.

[4] Misumi K, et al. (2014) The iron budget in ocean surface waters in the 20th and 21st centuries: projections by the Community Earth System Model version 1. *Biogeosci.* 11:33–55.

[5] Jickells TD, et al. (2005) Global iron connections between desert dust, ocean biogeochemistry, and climate. *Science* 308:67.

[6] Tagliabue A, et al. (2010) Hydrothermal contribution to the oceanic dissolved iron inventory. *Nat. Geosci.* 3:252–256.

[7] Sander SG, Koschinsky A (2011) Metal flux from hydrothermal vents increased by organic complexation. *Nat. Geosci.* 4:145–150.

[8] Saito MA, et al. (2013) Slow-spreading submarine ridges in the South Atlantic as a significant oceanic iron source. *Nat. Geosci.* 6:775–779.

[9] Severmann S, McManus J, Berelson WM, Hammond DE (2010) The continental shelf benthic iron flux and its isotope composition. *Geochim. Cosmochim. Acta* 74:3984–4004.

[10] Homoky WB, John SG, Conway TM, Mills RA (2013) Distinct iron isotopic signatures and supply from marine sediment dissolution. *Nat. Comm.* 4.

[11] Wu J, Boyle EA, Sunda W, Wen LS (2001) Soluble and colloidal iron in the oligotrophic North Atlantic and North Pacific. *Science* 293:847–849.

[12] Fung IY, et al. (2000) Iron supply and demand in the upper ocean. *Global Biogeochem. Cycles* 14:281–295.

[13] Moore JK, Doney SC, Glover DM, Fung IY (2001) Iron cycling and nutrient-limitation patterns in surface waters of the World Ocean. *Deep Sea Res. Part II* 49:463–507.

[14] Radic A, Lacan F, Murray JW (2011) Iron isotopes in the seawater of the equatorial Pacific Ocean: New constraints for the oceanic iron cycle. *Earth Planet. Sci. Lett.* 306:1–10.

[15] John SG, Adkins J (2012) The vertical distribution of iron stable isotopes in the North Atlantic near Bermuda. *Global Biogeochem. Cycles* 26.

[16] Conway TM, John SG (2014) Quantification of dissolved iron sources to the North Atlantic Ocean. *Nature* 511:212–215.

[17] Lacan F, et al. (2008) Measurement of the isotopic composition of dissolved iron in the open ocean. *Geophys. Res. Lett.* 35.

[18] Owens JD, et al. (2012) Iron isotope and trace metal records of iron cycling in the proto-North Atlantic during the Cenomanian-Turonian oceanic anoxic event (OAE-2). *Paleoceanography* 27.

[19] Frank M, O'Nions RK, Hein JR, Banakar VK (1999) 60 Myr records of major elements and Pb–Nd isotopes from hydrogenous ferromanganese crusts: Reconstruction of seawater paleochemistry. *Geochim. Cosmochim. Acta* 63:1689–1708.

[20] Hein JR, *et al.* (1987) *Farnella Cruise* F7-86-HW, Cobalt-rich Ferromanganese Crust Data Report for Karin Ridge and Johnston Island, Central Pacific., (US Geol. Surv.), Open File Rep. 87-663.

[21] Hein J, et al. (2000) in *Handbook of marine mineral deposits*, ed Cronan DS (CRC Press, Boca Raton, FL), pp 239–279.

[22] Koschinsky A, Hein JR (2003) Uptake of elements from seawater by ferromanganese crusts: solid-phase associations and seawater speciation. *Mar. Geol.* 198:331–351.

[23] Nielsen SG, et al. (2009) Thallium isotope evidence for a permanent increase in marine organic carbon export in the early Eocene. *Earth Planet. Sci. Lett.* 278:297–307.

[24] Bergquist BA, Wu J, Boyle EA (2007) Variability in oceanic dissolved iron is dominated by the colloidal fraction. *Geochim. Cosmochim. Acta* 71:2960–2974.

[25] Broecker WS, Peng TH (1982) *Tracers in the Sea* (Lamont-Doherty Geological Observatory, Columbia University), p 690.

[26] Henderson GM, Burton KW (1999) Using ($^{234}U/^{238}U$) to assess diffusion rates of isotope tracers in ferromanganese crusts. *Earth Planet. Sci. Lett.* 170:169–179.

[27] Hein JR, et al. (1993) Two major Cenozoic episodes of phosphogenesis recorded in equatorial Pacific seamount deposits. *Paleoceanography* 8:293–311.

[28] Chu NC, et al. (2006) Evidence for hydrothermal venting in Fe isotope compositions of the deep Pacific Ocean through time. *Earth Planet Sci. Lett.* 245:202–217.

[29] Janecek TR (1985) in *Deep Sea Drilling Project Leg 86, Western North Pacific*, Init. Repts. DSDP, ed Turner KL (U.S. Govt. Printing Office, Washington, D.C.) No. 19, pp 589–603.

[30] Janecek TR, Rea DK (1983) Eolian deposition in the northeast Pacific Ocean: Cenozoic history of atmospheric circulation. *Geol. Soc. Am. Bull.* 94:730–738.

[31] Schlitzer R (2011) Ocean Data View. (http://odv.awi.de/).

[32] Johnson CM, Beard BL, Albarède F (2004) *Geochemistry of non-traditional stable isotopes*, Rev. Mineral. Geochem. (Mineralogical Society of America, Washington, DC) Vol. 55.

[33] Levasseur S, Frank M, Hein JR, Halliday AN (2004) The global variation in the iron isotope composition of marine hydrogenetic ferromanganese deposits: implications for seawater chemistry? *Earth Planet. Sci. Lett.* 224:91–105.

[34] Johnson CM, Beard BL, Albarede F (2004) in *Geochemistry of non-traditional stable isotopes*, Rev. Mineral. Geochem., eds Johnson CM, Beard BL, Albarede F (Mineralogical Society of America) Vol. 55, pp 1–24.

[35] van den Berg CMG (1995) Evidence for organic complexation of iron in seawater. *Mar. Chem.* 50:139–157.

[36] Kraemer SM (2004) Iron oxide dissolution and solubility in the presence of siderophores. *Aquat. Sci.* 66:3–18.

[37] Dideriksen K, Baker J, Stipp SLS (2008) Fe isotope fractionation between inorganic aqueous Fe (III) and a Fe siderophore complex. *Min. Mag.* 72:313–316.

[38] Dideriksen K, Baker JA, Stipp SLS (2008) Equilibrium Fe isotope fractionation between inorganic aqueous Fe (III) and the siderophore complex, Fe (III)-desferrioxamine B. *Earth Planet. Sci. Lett.* 269:280–290.

[39] Morgan JLL, Wasylenki LE, Nuester J, Anbar AD (2010) Fe Isotope Fractionation during Equilibration of Fe- Organic Complexes. *Environ. Sci. Technol.* 44:6095–6101.

[40] Ryan BM, Kirby JK, Degryse F, Scheiderich K, McLaughlin MJ (2014) Copper Isotope Fractionation during Equilibration with Natural and Synthetic Ligands. *Environ. Sci. Technol.* 48:8620–8626.

[41] Little SH, Sherman DM, Vance D, Hein JR (2014) Molecular controls on Cu and Zn isotopic fractionation in Fe–Mn crusts. *Earth Planet. Sci. Lett.* 396:213–222.

[42] Barbeau K, Rue E, Bruland K, Butler A (2001) Photochemical cycling of iron in the surface ocean mediated by microbial iron (III)-binding ligands. *Nature* 413:409–413.

[43] Mawji E, et al. (2008) Hydroxamate siderophores: occurrence and importance in the Atlantic Ocean. *Environ. Sci. Technol.* 42:8675–8680.

[44] Rue EL, Bruland KW (1995) Complexation of iron (III) by natural organic ligands in the Central North Pacific as determined by a new competitive ligand equilibration/adsorptive cathodic stripping voltammetric method. *Mar. Chem.* 50:117–138.

[45] Cohen KM, Finney SC, Gibbard PL, Fan JX (2013) The ICS International Chronostratigraphic Chart. *Episodes* 36:199–204.

[46] Boyle EA (1997) What controls dissolved iron concentrations in the world ocean?—A comment. *Mar. Chem.* 57:163–167.

[47] Bennett SA, et al. (2008) The distribution and stabilisation of dissolved Fe in deep-sea hydrothermal plumes. *Earth Planet. Sci. Lett.* 270:157–167.

[48] Toner BM, et al. (2009) Preservation of iron(II) by carbon-rich matrices in a hydrothermal plume. *Nat. Geosci.* 2:197–201.

[49] Waeles M, Baker AR, Jickells T, Hoogewerff J (2007) Global dust teleconnections: aerosol iron solubility and stable isotope composition. *Environ. Chem.* 4:233–237.

[50] Beard BL, et al. (2003) Application of Fe isotopes to tracing the geochemical and biological cycling of Fe. *Chem. Geol.* 195:87–117.

[51] Severmann S, et al. (2004) The effect of plume processes on the Fe isotope composition of hydrothermally derived Fe in the deep ocean as inferred from the Rainbow vent site, Mid-Atlantic Ridge, 36°14'N. *Earth Planet. Sci. Lett.* 225:63–76.

[52] Rouxel O, Shanks III WC, Bach W, Edwards KJ (2008) Integrated Fe-and S-isotope study of seafloor hydrothermal vents at East Pacific Rise 9–10 N. *Chem. Geol.* 252:214–227.

[53] Wiederhold JG, et al. (2006) Iron isotope fractionation during proton-promoted, ligand-controlled, and reductive dissolution of goethite. *Environ. Sci. Technol.* 40:3787–3793.

[54] Butler IB, Archer C, Vance D, Oldroyd A, Rickard D (2005) Fe isotope fractionation on FeS formation in ambient aqueous solution. *Earth Planet. Sci. Lett.* 236:430–442.

[55] Severmann S, Johnson CM, Beard BL, McManus J (2006) The effect of early diagenesis on the Fe isotope compositions of porewaters and authigenic minerals in continental margin sediments. *Geochim. Cosmochim. Acta* 70:2006–2022.

[56] Guilbaud R, Butler IB, Ellam RM (2011) Abiotic pyrite formation produces a large Fe isotope fractionation. *Science* 332:1548–1551.

[57] Bennett SA, et al. (2009) Iron isotope fractionation in a buoyant hydrothermal plume, 5 S Mid-Atlantic Ridge. *Geochim. Cosmochim. Acta* 73:5619–5634.

[58] Aquilina A, et al. (2013) Diagenetic Mobilisation of Fe and Mn in Hydrothermal Sediments. *Min. Mag.* 77:604.

[59] Klemm V, Reynolds B, Frank M, Pettke T, Halliday AN (2007) Cenozoic changes in atmospheric lead recorded in central Pacific ferromanganese crusts. *Earth Planet. Sci. Lett.* 253:57–66.

[60] Van Andel TH, Heath GR, Moore TC (1975) Cenozoic History and Paleoceanography of the Central Equatorial Pacific Ocean A Regional Synthesis of Deep Sea Drilling Project Data. *Geol. Soc. Am. Mem.* 143:1–223.

[61] Cogné JP, Humler E (2006) Trends and rhythms in global seafloor generation rate. *Geochem. Geophys. Geosyst.* 7:Q03011.

[62] Von Damm KL, et al. (1985) Chemistry of submarine hydrothermal solutions at 21 °N, East Pacific Rise. *Geochim. Cosmochim. Acta* 49:2197–2220.

[63] Wu J, Wells ML, Rember R (2011) Dissolved iron anomaly in the deep tropical–subtropical Pacific: Evidence for long-range transport of hydrothermal iron. *Geochim. Cosmochim. Acta* 75:460–468.

[64] Fitzsimmons JN, Boyle EA, Jenkins WJ (2014) Distal transport of dissolved hydrothermal iron in the deep South Pacific Ocean. *Proc. Natl. Acad. Sci.* p 201418778.

[65] Lupton J (1998) Hydrothermal helium plumes in the Pacific Ocean. *J. Geophys. Res.* 103:15853–15868.

[66] Reid JL (1997) On the total geostrophic circulation of the Pacific Ocean: Flow patterns, tracers, and transports. *Prog. Oceanogr.* 39:263–352.

[67] John SG, Mendez J, Moffett J, Adkins J (2012) The flux of iron and iron isotopes from San Pedro Basin sediments. *Geochim. Cosmochim. Acta* 93:14–29.

[68] Lam PJ, Bishop JK (2008) The continental margin is a key source of iron to the HNLC North Pacific Ocean. *Geophys. Res. Lett.* 35.

[69] Bruland KW, Rue EL, Smith GJ, DiTullio GR (2005) Iron, macronutrients and diatom blooms in the Peru upwelling regime: brown and blue waters of Peru. *Mar. Chem.* 93:81–103.

[70] Stramma L, Schmidtko S, Levin LA, Johnson GC (2010) Ocean oxygen minima expansions and their biological impacts. *Deep Sea Res. Part I* 57:587–595.

[71] Davis AS, Gray LB, Clague DA, Hein JR (2002) The Line Islands revisited: New $^{40}Ar/^{39}Ar$ geochronologic evidence for episodes of volcanism due to lithospheric extension. *Geochem. Geophys. Geosyst.* 3:1–28.

[72] Hein JR, *et al.* (1990) Geological, geochemical, geophysical, and oceanographic data and interpretations of seamounts and Co-rich ferromanganese crusts from the Marshall Islands, KORDI-USGS RV *Farnella* cruise F10-89-CP., (US Geol. Surv.), Open File Rep. 90-407.

[73] Parsons B, Sclater JG (1977) An analysis of the variation of ocean floor bathymetry and heat flow with age. *J. Geophys. Res.* 82:803–827.

[74] Klemm V, Levasseur S, Frank M, Hein JR, Halliday AN (2005) Osmium isotope stratigraphy of a marine ferromanganese crust. *Earth Planet. Sci. Lett.* 238:42–48.

[75] Williams HM, et al. (2005) Systematic iron isotope variations in mantle rocks and minerals: the effects of partial melting and oxygen fugacity. *Earth Planet. Sci. Lett.* 235:435–452.

[76] Williams HM, et al. (2009) Fractionation of oxygen and iron isotopes by partial melting processes: implications for the interpretation of stable isotope signatures in mafic rocks. *Earth Planet. Sci. Lett.* 283:156–166.

[77] Mikutta C, et al. (2009) Iron isotope fractionation and atom exchange during sorption of ferrous iron to mineral surfaces. *Geochim. Cosmochim. Acta* 73:1795–1812.

[78] Dideriksen K, Baker JA, Stipp SLS (2006) Iron isotopes in natural carbonate minerals determined by MC-ICP-MS with a ^{58}Fe–^{54}Fe double spike. *Geochim. Cosmochim. Acta* 70:118–132.

[79] Weyer S, et al. (2005) Iron isotope fractionation during planetary differentiation. *Earth Planet. Sci. Lett.* 240:251–264.

[80] David K, Frank M, O'Nions RK, Belshaw NS, Arden JW (2001) The Hf isotope composition of global seawater and the evolution of Hf isotopes in the deep Pacific Ocean from Fe–Mn crusts. *Chem. Geol.* 178:23–42.

[81] Johnson KS, Gordon RM, Coale KH (1997) What controls dissolved iron concentrations in the world ocean? *Mar. Chem.* 57:137–161.

[82] Burrell M, Hanfrey CC, Kinch LN, Elliott KA, Michael AJ (2012) Evolution of a novel lysine decarboxylase in siderophore biosynthesis. *Mol. Microbiol.* 86:485–499.

[83] Ehmann DE, Shaw-Reid CA, Losey HC, Walsh CT (2000) The EntF and EntE adenylation domains of *Escherichia coli* enterobactin synthetase: Sequestration and selectivity in acyl-AMP transfers to thiolation domain cosubstrates. *Proc. Natl. Acad. Sci.* 97:2509–2514.

[84] Yamanaka K, et al. (2005) Desferrioxamine E produced by *Streptomyces griseus* stimulates growth and development of *Streptomyces tanashiensis*. *Microbiol.* 151:2899–2905.

[85] Altschul SF, Gish W, Miller W, Myers EW, Lipman DJ (1990) Basic local alignment search tool. *J. Mol. Biol.* 215:403–410.

[86] Feng DF, Doolittle RF (1997) Converting amino acid alignment scores into measures of evolutionary time: a simulation study of various relationships. *J. Mol. Evo.* 44:361–370.

[87] Grishin NV (1995) Estimation of the number of amino acid substitutions per site when the substitution rate varies among sites. *J. Mol. Evo.* 41:675–679.

[88] Feng DF, Cho G, Doolittle RF (1997) Determining divergence times with a protein clock: Update and reevaluation. *Proc. Natl. Acad. Sci.* 94:13028–13033.

[89] Ochman H, Elwyn S, Moran NA (1999) "Calibrating bacterial evolution". *Proc. Natl. Acad. Sci.* 96:12638–12643.

[90] Benjamin WH, Turnbough CL, Posey BS, Briles DE (1985) The ability of *Salmonella typhimurium* to produce the siderophore enterobactin is not a virulence factor in mouse typhoid. *Infect. Immun.* 50:392–397.

[91] Christensen JN, Halliday AN, Godfrey LV, Hein JR, Rea DK (1997) Climate and ocean dynamics and the lead isotopic records in Pacific ferromanganese crusts. *Science* 277:913.

[92] Pälike H, *et al.* (2012) A Cenozoic record of the equatorial Pacific carbonate compensation depth. *Nature* 488:609–614.

[93] Zachos J, Pagani M, Sloan L, Thomas E, Billups K (2001) Trends, rhythms, and aberrations in global climate 65 Ma to present. *Science* 292:686–693.

[94] Pagani M, et al. (2011) The role of carbon dioxide during the onset of Antarctic glaciation. *Science* 334:1261–1264.

[95] Boyle EA, Bergquist BA, Kayser RA, Mahowald N (2005) Iron, manganese, and lead at Hawaii Ocean Time-series station ALOHA: Temporal variability and an intermediate water hydrothermal plume. *Geochim. Cosmochim. Acta* 69:933–952.

[96] Tagliabue A, Aumont O, Bopp L (2014) The impact of different external sources of iron on the global carbon cycle. *Geophys. Res. Lett.* 41:920–926.

[97] Douville E, et al. (2002) The rainbow vent fluids (36 14? n, mar): the influence of ultramafic rocks and phase separation on trace metal content in mid-atlantic ridge hydrothermal fluids. *Chem. Geol.* 184:37–48.

[98] Mottl MJ, McConachy TF (1990) Chemical processes in buoyant hydrothermal plumes on the east pacific rise near 21 n. *Geochim. Cosmochim. Acta* 54:1911–1927.

[99] Fitzsimmons J, Conway T, John SG, Boyle EA (2013) Iron Isotopes in Seawater from the Southeast Pacific and North Atlantic Oceans. *Min. Mag.* 77:1092.

[100] Lupton JE, Craig H (1981) A Major Helium-3 Source at 15°S on the East Pacific Rise. *Science* 214:13–18.

[101] Rijkenberg MJ, et al. (2014) The Distribution of Dissolved Iron in the West Atlantic Ocean. *PloS One* 9:e101323.

[102] Nishioka J, Obata H, Tsumune D (2013) Evidence of an extensive spread of hydrothermal dissolved iron in the Indian Ocean. *Earth Planet. Sci. Lett.* 361:26–33.

[103] Toner BM, Marcus MA, Edwards KJ, Rouxel O, German CR (2012) Measuring the form of iron in hydrothermal plume particles. *Oceanogr.* 25:209–212.

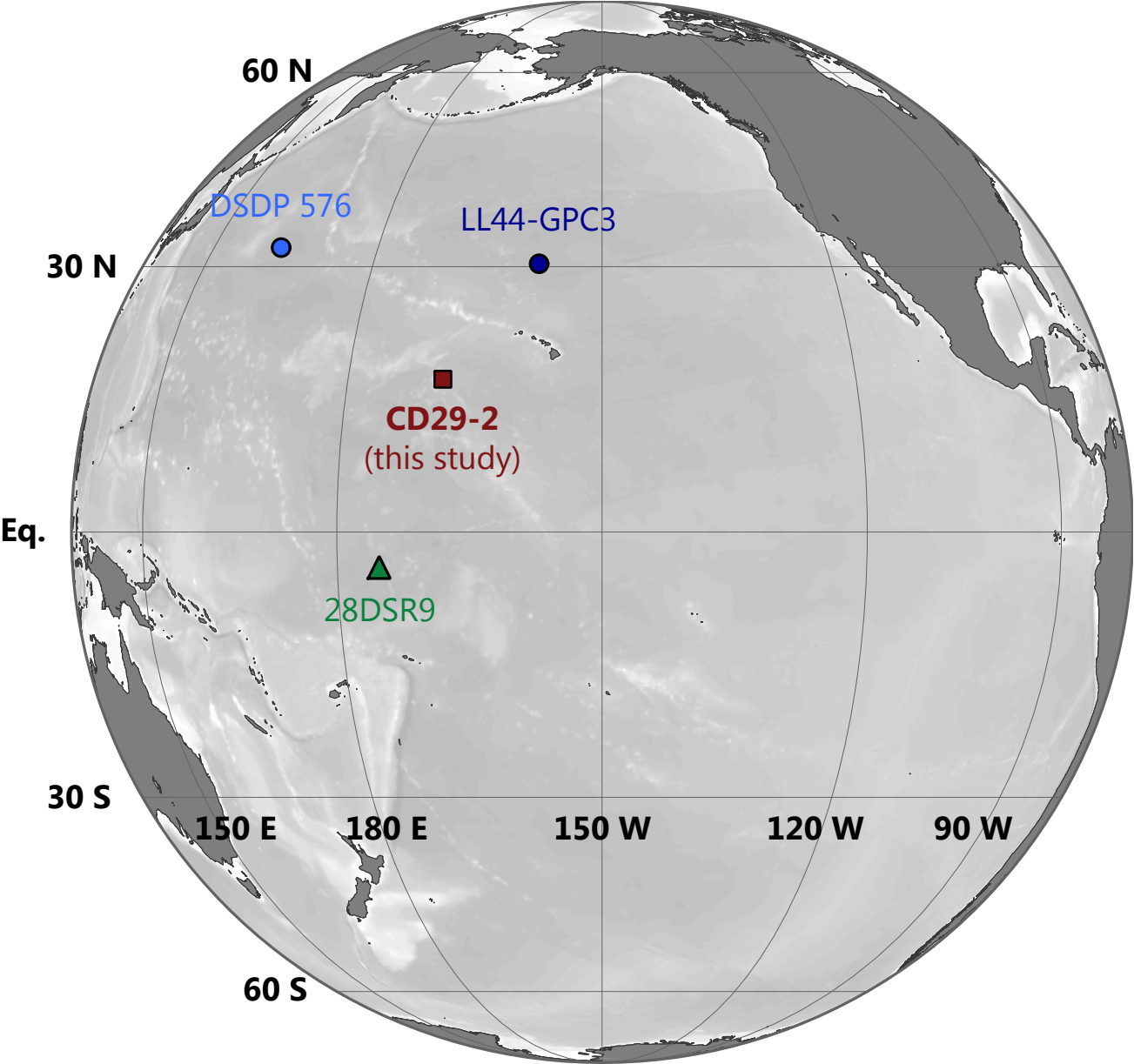
60 N
30 N
Eq.
30 S
60 S
150 E
180 E
150 W
120 W
90 W
DSDP 576
LL44-GPC3
CD29-2
(this study)
28DSR9

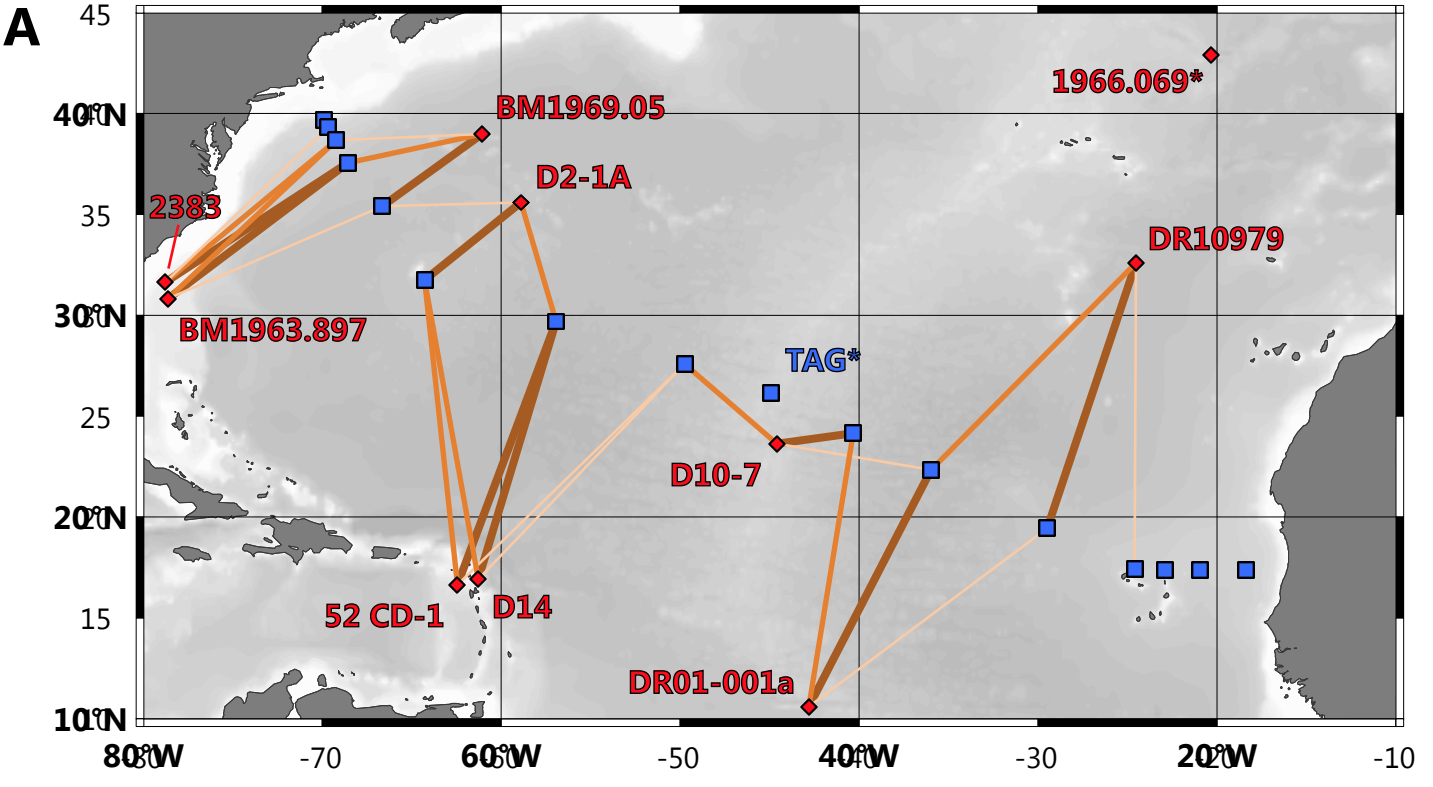
A
45
40°N
35
30°N
25
20°N
15
10°N
80°W
-70
60°W
-50
40°W
-30
20°W
-10
BM1969.05
1966.069*
D2-1A
2383
DR10979
BM1963.897
TAG*
D10-7
52 CD-1
D14
DR01-001a

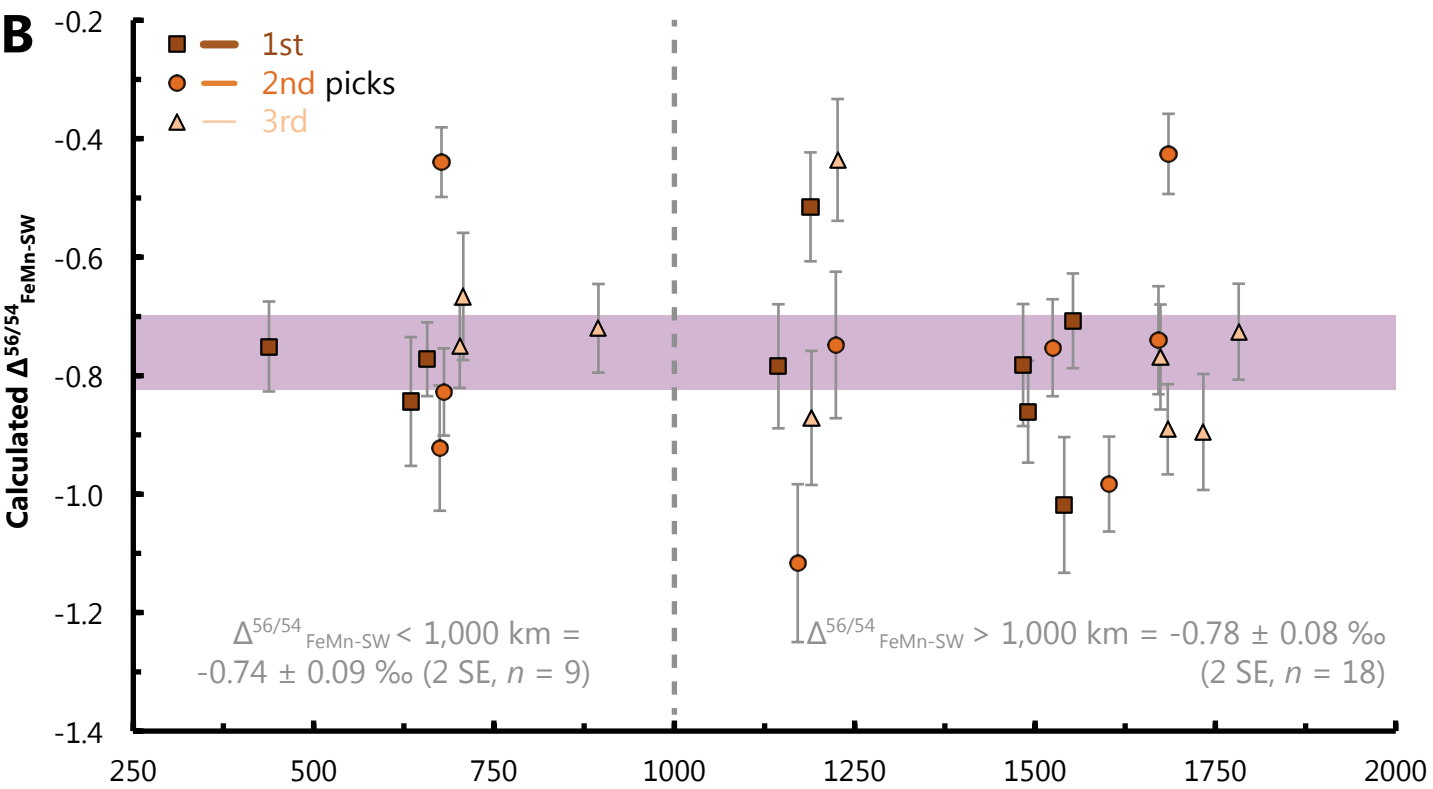
B
1st
2nd picks
3rd
Calculated Δ56/54FeMn-SW
-0.2
-0.4
-0.6
-0.8
-1.0
-1.2
-1.4
Δ56/54FeMn-SW < 1,000 km =
-0.74 ± 0.09 ‰ (2 SE, n = 9)
Δ56/54FeMn-SW > 1,000 km = -0.78 ± 0.08 ‰
(2 SE, n = 18)
250
500
750
1000
1250
1500
1750
2000

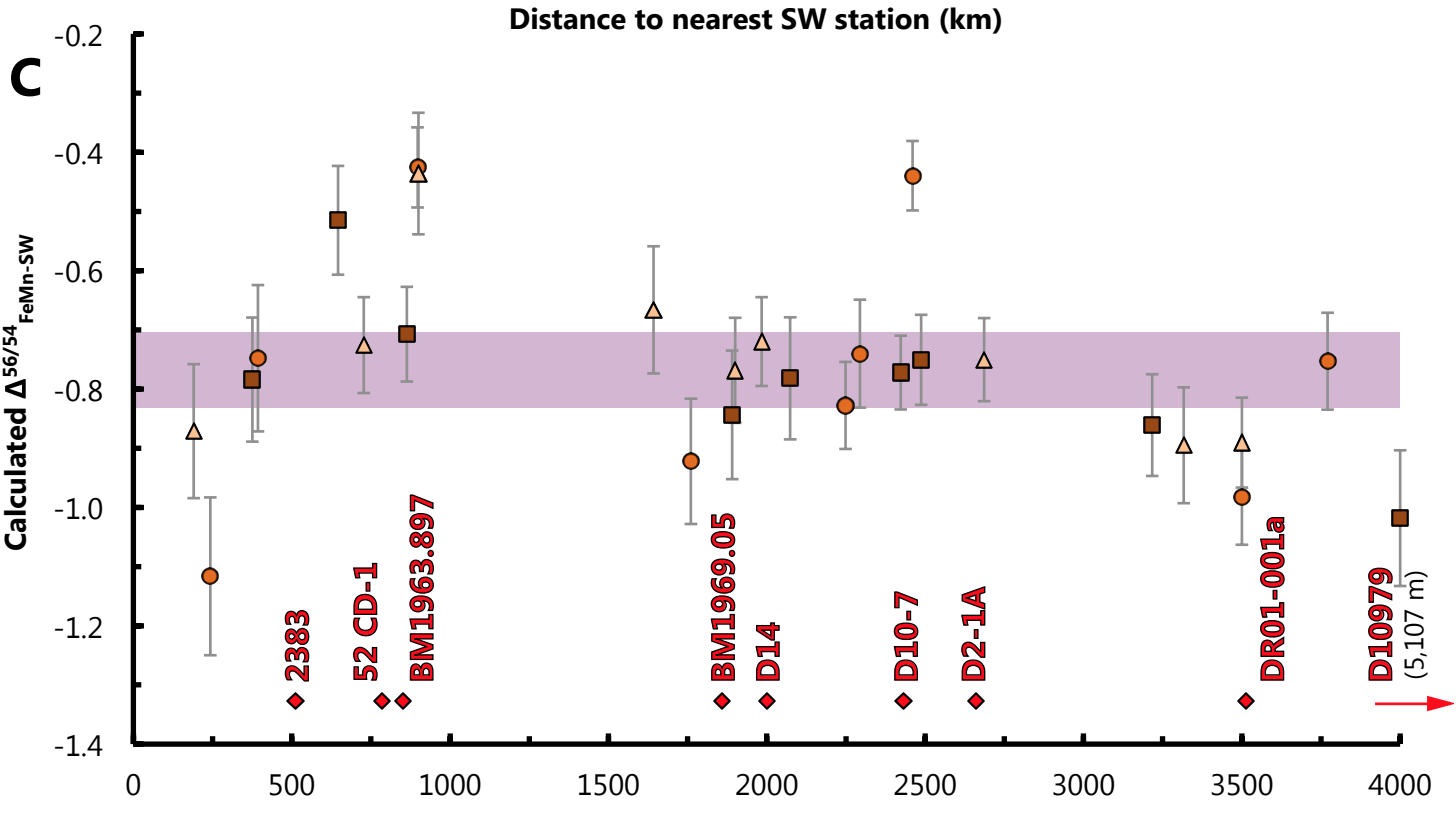
C
Distance to nearest SW station (km)
Calculated Δ56/54FeMn-SW
-0.2
-0.4
-0.6
-0.8
-1.0
-1.2
-1.4
2383
52 CD-1
BM1963.897
BM1969.05
D14
D10-7
D2-1A
DR01-001a
D10979
(5,107 m)
0
500
1000
1500
2000
2500
3000
3500
4000
Depth at corresponding density surface (m)

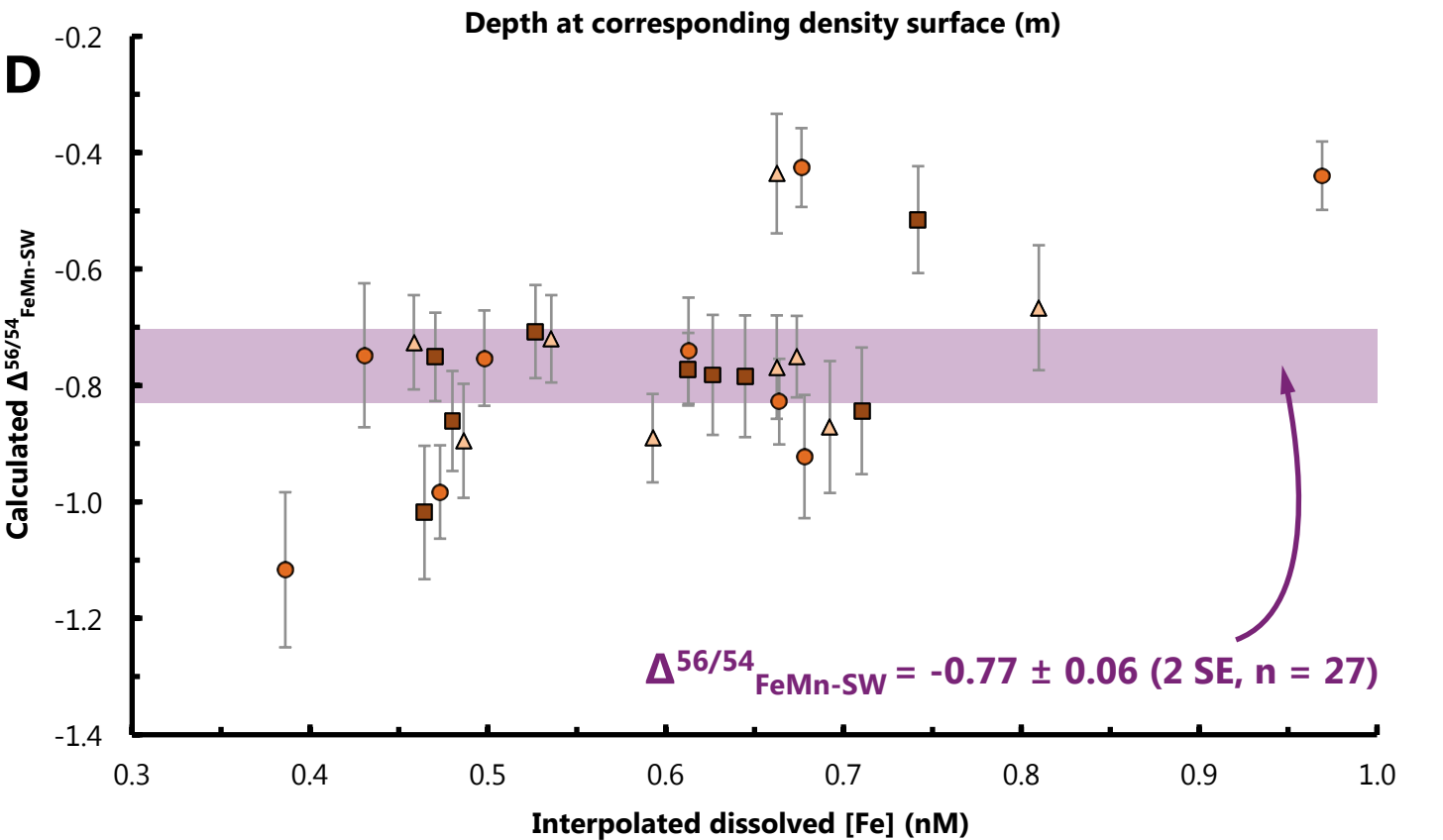
D
Calculated Δ56/54FeMn-SW
-0.2
-0.4
-0.6
-0.8
-1.0
-1.2
-1.4
Δ56/54FeMn-SW = -0.77 ± 0.06 (2 SE, n = 27)
0.3
0.4
0.5
0.6
0.7
0.8
0.9
1.0
Interpolated dissolved [Fe] (nM)

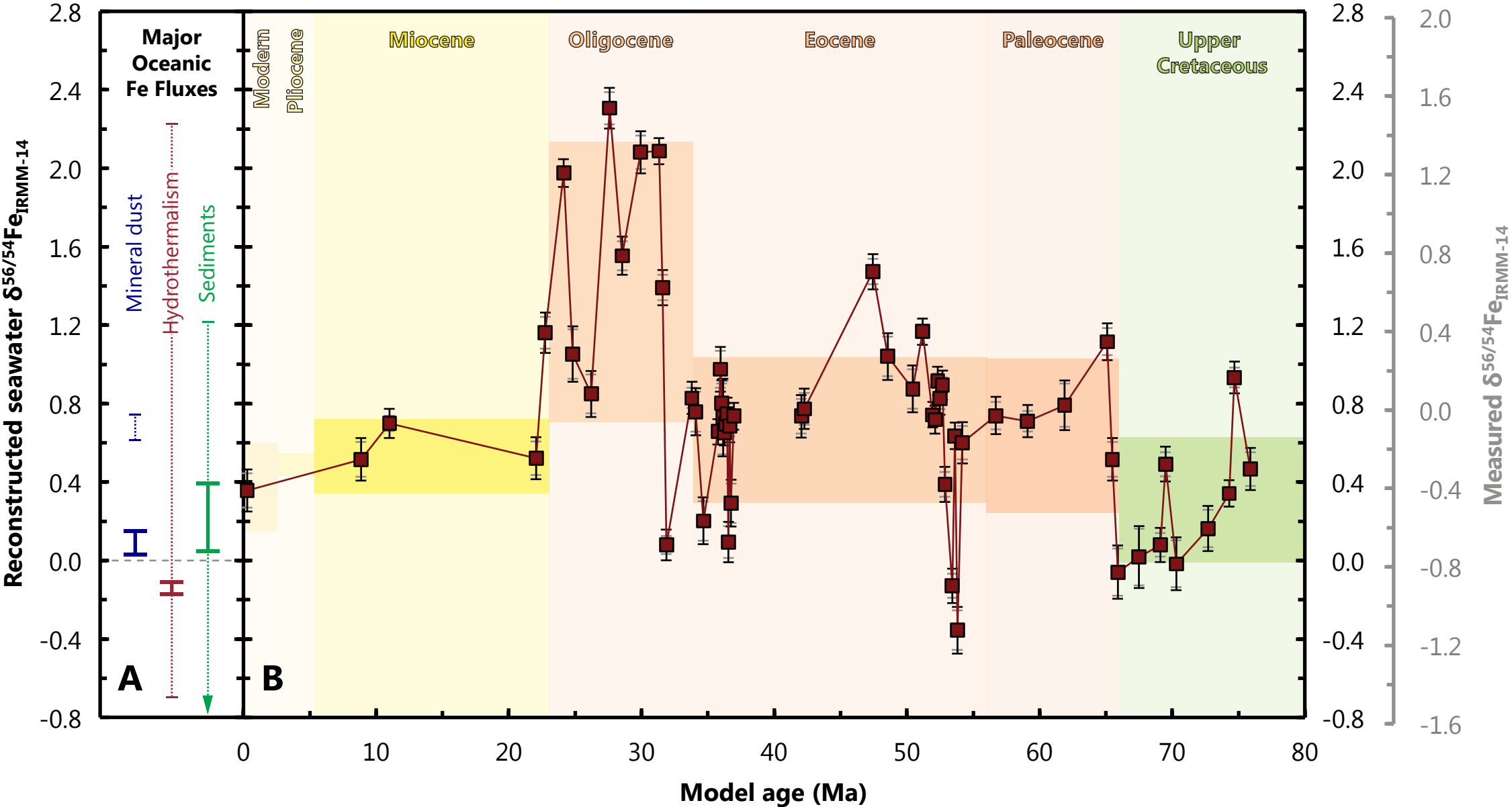
Major Oceanic Fe Fluxes
Mineral dust
Hydrothermalism
Sediments
A
B
Modern
Pliocene
Miocene
Oligocene
Eocene
Paleocene
Upper Cretaceous
Reconstructed seawater δ56/54FeIRMM-14
Measured δ56/54FeIRMM-14
Model age (Ma)
2.8
2.4
2.0
1.6
1.2
0.8
0.4
0.0
-0.4
-0.8
2.0
1.6
1.2
0.8
0.4
0.0
-0.4
-0.8
-1.2
-1.6
0
10
20
30
40
50
60
70
80

Model age (Ma)

0 10 20 30 40 50 60 70 80

A

B

C

D

Reconstructed seawater $\delta^{56/54}Fe_{IRMM-14}$

2.8 2.4 2.0 1.6 1.2 0.8 0.4 0.0 -0.4 -0.8

CD29-2 latitude (°)

20 10 0 -10

Inferred Fe-isotopic composition of dust

DSDP 576 or LL44-GPC3 eolian MAR (mg cm^{-2} kyr^{-1})

5000 500 50 5

Pacific Plate dA/dt (km^2 100 yr^{-1}) or spreading rate (mm yr^{-1})

200 150 100 50 0

0 10 20 30 40 50 60 70 80

Model age (Ma)

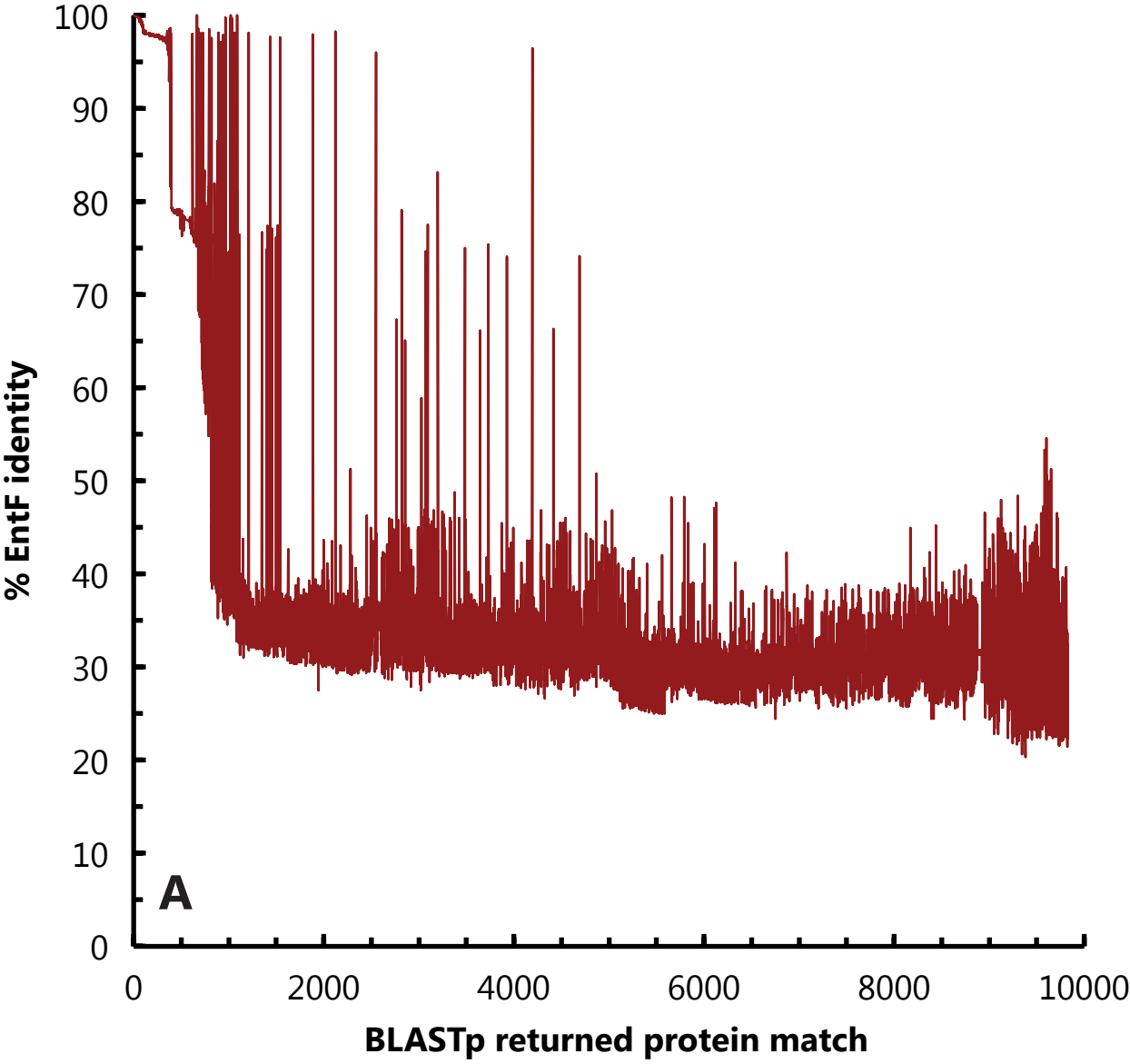
% EntF identity
100
90
80
70
60
50
40
30
20
10
0
A
0
2000
4000
6000
8000
10000
BLASTp returned protein match

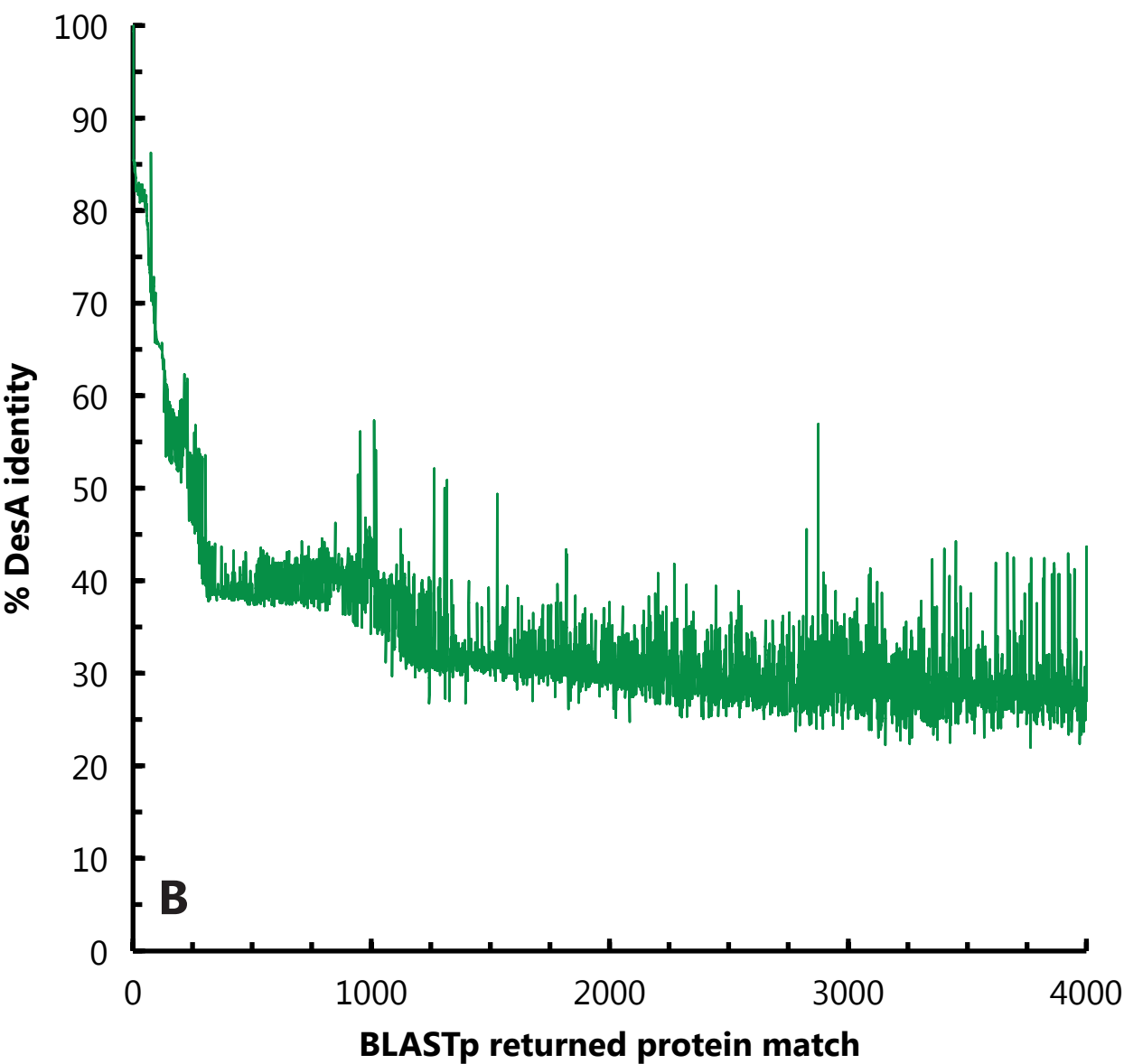
% DesA identity
100
90
80
70
60
50
40
30
20
10
0
B
0
1000
2000
3000
4000
BLASTp returned protein match

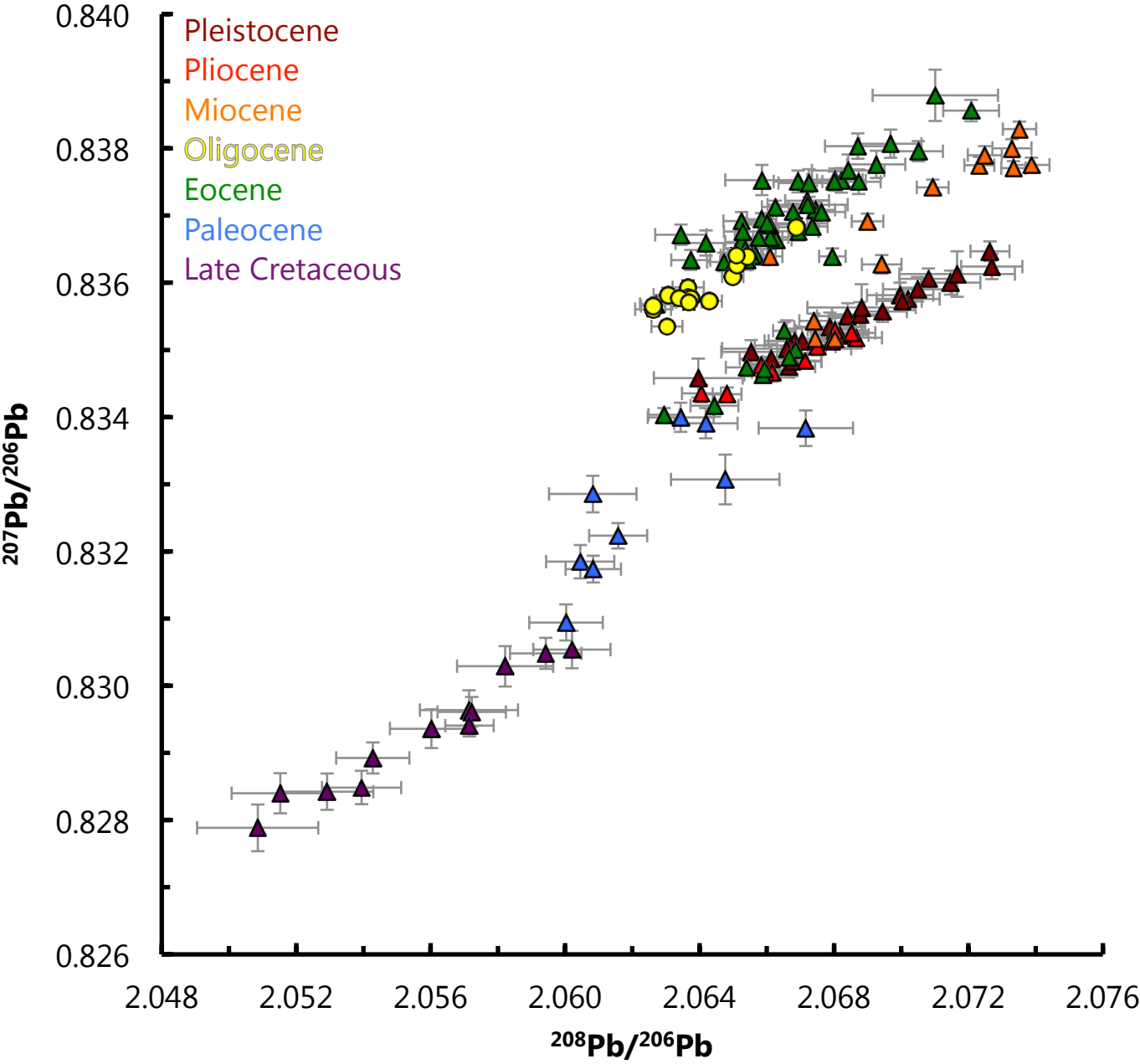
Pleistocene
Pliocene
Miocene
Oligocene
Eocene
Paleocene
Late Cretaceous
0.840
0.838
0.836
0.834
0.832
0.830
0.828
0.826
$^{207}Pb/^{206}Pb$
2.048
2.052
2.056
2.060
2.064
2.068
2.072
2.076
$^{208}Pb/^{206}Pb$